POLITECNICO DI TORINO
Repository ISTITUZIONALE

Energy performance of Power-to-Liquid applications integrating biogas upgrading, reverse water gas shift, solid oxide electrolysis and Fischer-Tropsch technologies

(Article begins on next page)
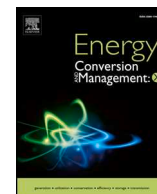
01 September 2025

Energy performance of Power-to-Liquid applications integrating biogas upgrading, reverse water gas shift, solid oxide electrolysis and Fischer-Tropsch technologies

Marco Marchese[a,*], Emanuele Giglio[a,b], Massimo Santarelli[a], Andrea Lanzini[a]

[a] Energy Department, Politecnico di Torino, Corso Duca degli Abruzzi 24, 10129 Torino, Italy
[b] Department of Environmental Engineering, University of Calabria, Via Pietro Bucci, 87036 Rende, CS, Italy

ARTICLE INFO

ABSTRACT

Power-to-liquid (P2L) pathways represent a possible solution for the conversion of carbon dioxide into synthetic value-added products. The present work analyses different power-to-liquid options for the synthesis of Fischer-Tropsch (FT) fuels and chemicals. The FT section is integrated into a complete carbon capture and utilization route. The involved processes are a biogas upgrading unit for CO_2 recovery, a reverse water gas shift, a solid oxide electrolyser and a Fischer-Tropsch reactor.

The upgrading plant produces about 1 ton/h of carbon dioxide. The recovered CO_2 is fed to either a reverse water gas shift reactor or a solid oxide electrolysis unit operating in co-electrolysis mode for the generation of syngas. The produced syngas is fed to a Fischer-Tropsch reactor at 501 K and 25 bar for the synthesis of the Fischer-Tropsch products, which are further separated into different classes based on their boiling point to yield light gas, naphtha, middle distillates, light waxes and heavy waxes. The developed process model uses a detailed carbide kinetic model to describe the formation of paraffins and olefins based on real experimental data. The effect of Fischer-Tropsch off-gas recirculation has been studied against a one-through option. Finally, energy integration of each configuration plant is provided. Results from process simulations show that the best model configurations reach a plant efficiency of 81.1% in the case of solid oxide electrolyser as syngas generator, and 71.8% in the case of reverse water gas shift option, with a global carbon reduction potential of 79.4% and 81.7%, respectively.

1. Introduction

Since the Paris agreement of the COP21, increasing effort has been spent in implementing solutions that can reduce greenhouse gases emissions towards the environment. Thus, alongside the deployment of renewable energy technologies, the study of novel applications that can store such energy meanwhile utilizing CO_2 of industrial processes as raw material has gained much attention [1].

Means for on-site carbon dioxide reuse include power-to-gas (P2G) and power-to-liquid (P2L) applications. These concepts consider exploiting CO_2 as a useful commodity, shifting it from a low-value resource to high-value product, meanwhile storing energy from renewable electricity [2,3]. In the framework of P2G and P2L routes, different steps are required to transform carbon dioxide into further products. CO_2 can be captured from the flue gas of industrial and energy plants burning fossil fuels through highly energy-intensive chemical or physical capture processes, upgrading of biogas, or even from the air with direct air capture technologies (DAC) [4–6]. Furthermore, the captured molecule can be transformed into synthetic products through thermochemical or electrochemical processes. These processes enable methane and syngas synthesis in the case of P2G, while P2L final outcomes can include Fischer-Tropsch fuels and chemicals, methanol, dimethyl ether (DME) and formic acid [7–9].

In the present work, we focus on P2L chains presenting a Fischer-Tropsch reactor (FT). The FT technology has risen in scientific interest as an effective application to be inserted into carbon capture and utilization (CCU) plants, capable of delivering the so-called syncrude [10]: a broad mixture of synthetic hydrocarbons that can replace oil extracted from the ground. Syncrude accounts for hydrocarbons ranging from carbon number C_1 to C_{80+}, in the form of n-paraffins, α-olefins, with a lower content of alcohols and aromatic compounds [11]. Hence, the great potential of the FT processes is the displacement opportunity

---

Nomenclature

A	Area (cm^2)
F	Faraday constant (C mol_e^{-1})
I	Current (A)
j	Current density (A cm^{-2})
K	Equilibrium constant
k	Kinetic constant
n	Carbon number
$\dot{n}_{i\text{-th}}$	Mole flow rate of component i-th (mol s^{-1})
n_{tot}	Exchange charge
P	Pressure (bar)
R	Gas constant (kJ $kmol^{-1}$ K^{-1})
T	Temperature (K)
V	Voltage (V)
W	Power (W)
α	Hydrocarbon probability growth
ΔG	Gibbs free energy (kJ $kmol^{-1}$)
ΔH	Enthalpy change
Δp	Pressure variation
ΔT	Temperature variation
η	Efficiency
Θ	Vacancy percentage
X	Conversion

Abbreviations

ASR	Area-specific resistance (Ωcm^2)
ATR	Auto thermal reactor
CCU	Carbon capture and utilization
CGO	Gallium-doped ceria
CPOX	Partial oxidation
CRP	Carbon reduction potential
DAC	Direct air capture
FT	Fischer-Tropsch
LHV	Low Heating Value
LSC	Lanthanum strontium cobaltite
MEA	Monoethanolamine
Ni	Nickel
OCV	Open circuit voltage
P2G	Power to gas
P2L	Power to liquid
RR	Recirculation rate
RU	Reactant utilization
RWGS	Reverse water gas shift
SMR	Steam methane reforming
SOE	Solid oxide electrolyser
SOEC	Solid oxide electrolysis cell
TN	Thermoneutral
YSZ	Yttria-stabilized zirconia

of wide-ranging hydrocarbons of fossil origin. Transportation sector utilizing gasoline, diesel and jet fuels, and the chemical industry utilizing long-chain hydrocarbons as a feedstock for chemical products can be inserted into a circular economy concept, where the use of fossil material is avoided in favour of recycled CO_2 [12,13].

The input to the Fischer-Tropsch process is synthesis gas, namely syngas that is a mixture of CO_2, H_2, CO and H_2O mainly. To obtain it, the captured carbon dioxide can be converted into CO through thermochemical or electrochemical devices. Thus, reverse water gas shift reactors (RWGS), autothermal reactors (ATR), partial oxidation reactors (CPOX), steam methane reformers (SMR) or solid oxide electrolysis cells (SOEC) can be employed. Specifically, RWGS and SOEC can directly convert carbon dioxide to CO with the aid of hydrogen or steam, whereas CPOX, ATR and SMR use methane (or other hydrocarbons) for the syngas generation [14,15].

Once the syngas is fed to the Fischer-Tropsch reactor, the description of the FT products distribution becomes a key aspect in evaluating the whole system performance. Different kinetic approaches can be used. The overall FTS synthesis can be described by a single equation like a modification of the Anderson-Flory-Shultz theory or power-law kinetics [16]. Selectivity models can provide information on the reactants consumption rates and specific groups of FT compounds [17]. Finally, mechanistic kinetic models allow for the identification of reactants consumption rates as well as products generation rates. A recent review comprising the FT kinetics, beyond the scope of this work, is provided by Santos et al. [18]. A different amount of information can be extracted from the PtL models, depending on the modelling approach employed for the FTS. For instance, Cinti et al. [19] applied in their work on SOEC + FT the AFS distribution at a fixed chain growth probability α = 0.94, with a modification to account for olefins and paraffins formation. In this regard, they could identify 5 main molecules representative of the paraffins, 4 for the olefins and a clustered molecule to account for C_{30+} waxes. Fazeli et al. [20] employed a one-step reaction rate to describe the FT synthesis, with weight distribution based on lumped species experimental data. Selvatico et al. [21], instead, used detailed kinetics for olefins and paraffins, but only up to carbon number C_{30}, thus excluding the heaviest FT fractions of interest if targeting long-chain hydrocarbons like C_{30+} waxes.

As far as P2L routes are concerned, different solutions have been proposed in literature. Herz et al. [22] created a possible SOEC + FT process model with SOE stacks operating in co-electrolysis mode, calculating a maximum process efficiency of 68.1%. Rafiee et al. [23] reached a carbon efficiency (i.e., efficiency of carbon utilization) of 68.2% for a system that captured CO_2 from flue gases, combining it together with an ATR and an FT reactor. Vidal et al. [24] studied the integration of a DAC with low temperature electrolysis, RWGS and FT reactors, reaching 94% carbon efficiency and 47% plant efficiency. In fact, different studies on the integration of FT reactors with syngas generation units for P2L systems can be found. However, to the best of our knowledge, not many studies include a full process integrated with the carbon capture one, and seldom focusing on a detailed products separation analysis, too. For instance, Tagomori et al. [25] stated the need of properly designing and evaluating the process of distillation of the FT products.

In the present work, we provide a P2L system analysis from the capture of CO_2 to the generation and separation of the synthetic products. We investigate the coupling between a solvent-based biogas upgrading process and the Fischer-Tropsch reactor with two concurrent technologies for syngas generation: one proven and commercially available technology like the RWGS reactor; one less commercialized technology but with high CO_2 conversion potential like the SOEC under co-electrolysis. To the authors knowledge, only one report (Comidy et al. [26]) is available in the open literature that provides some insight on the direct comparison of a P2L with RWGS against a P2L with SOEC technologies feeding a Fischer-Tropsch reactor. However, their analysis focused on the production of light FT fuels for on-board consumption on aircraft carriers. Furthermore, they stated that no experimental validation of any of their employed technologies was assessed. In this work, we include a mechanistic kinetic description based on the carbide FTS mechanisms of paraffins and olefins up to carbon number C_{80}, experimentally validated for the Fischer-Tropsch reactor and presented in another research work (Marchese et al. [27]). Specifically, the model provides detailed information about the production rate of each of the heaviest FT fraction compounds, that are generally clustered into one single C_{30+} pseudo-component [21], from which exact FTS heat of reaction is evaluated. Finally, our model includes in the analysis two

distillation towers: the first needed to separate waxes, the second to distillate the lighter FT products. With this work, we seek to maximize the synthesis of middle distillates and waxes fractions, maximize the CO_2 conversion and minimize the thermal requirements of the process. Each system is thermally integrated allowing a sensible reduction in the thermal energy needs of the highly energy-intensive MEA process. Lastly, considerations about the technology readiness level of each device are given.

2. Methodology

2.1. Plant layout

A biogas upgrading unit based on chemical scrubbing and separating CO_2 from CH_4 was chosen as the source for carbon dioxide. Two different process configurations were then studied, with variation in the syngas generation unit. The recovered CO_2 from the biogas upgrading section was fed to either an RWGS reactor or a SOEC stack operating under co-electrolysis conditions for the synthesis gas generation. In the

case of the RWGS solution, a low-temperature electrolysis unit was also inserted to deliver the required hydrogen for the process. The resulting syngas was dehydrated and supplied to a Fischer-Tropsch reactor for the syncrude synthesis. The syncrude was further upgraded into several chemical classes, based on their boiling point: gas, naphtha, middle distillates, light waxes and heavy waxes. To increase the targeted Fisher-Tropsch products yield, each configuration also accounted for a recirculation solution of the Fischer-Tropsch off-gases back to the syngas generation unit inlet. The conditions at 0% recirculation rate (0% RR) of the off-gases were considered as the reference. Finally, the effect of gas pressurization before the RWGS and the SOEC was additionally included in the analysis. The model was developed on the commercial tool for mass and energy balances AspenPLUS™. Fig. 1 depicts schematics of analysed processes.

2.2. Biogas upgrading and CO_2 capture unit

The first unit (common to all the plant configurations) consisted of a medium-size biogas-upgrading system, which disposed of 1680 m³/hr
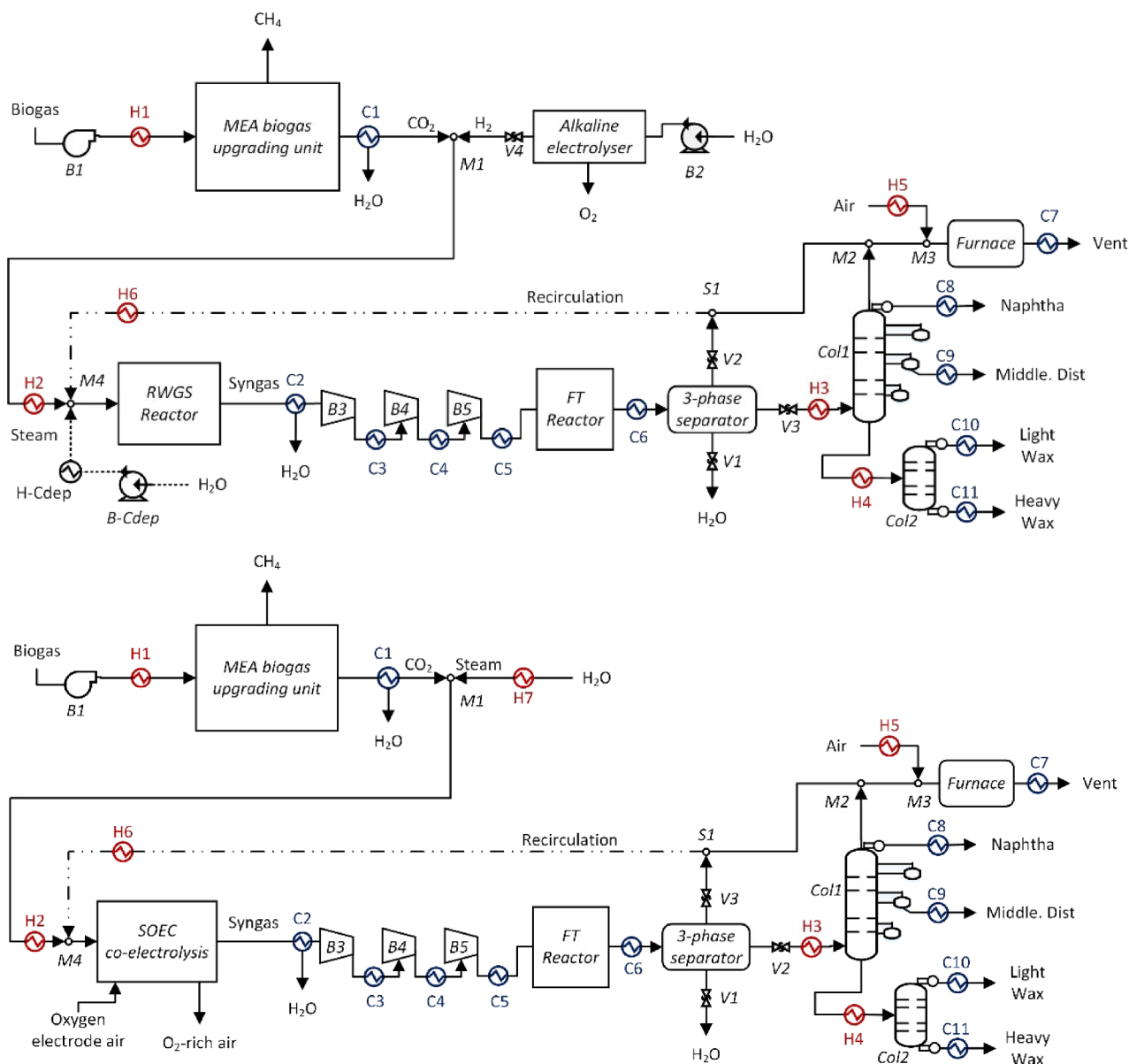

Fig. 1. Plant layouts from biogas inlet to FT products separation: top) Case A with RWGS reactor for syngas generation; bottom) Case B with SOEC stack for syngas generation.
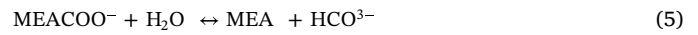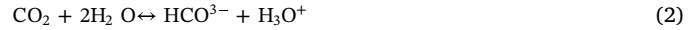
of clean biogas, with 34 mol-% CO_2, 65 mol-% CH_4 and 1 mol-% N_2, resulting in 1 ton/hr of CO_2 captured [28]. The solvent selected for the absorption process was monoethanolamine (MEA). A detailed layout of this biogas upgrading process is presented in Fig. 2. The absorber was modelled as a rate-based multistage packing column, where the solvent amine selectively bound with the CO_2 in the biogas stream via an exothermic reaction. The stripper was a rate-based multistage packing column, where the release of the CO_2 took place by means of heat transfer through the reboiler bottom stage. The make-up section allowed for the reintegration of MEA and water lost during the process of separation. The cross heat exchanger preheated the CO_2-rich stream entering the stripper while precooling the one exiting the stripper. A minimum temperature difference of 15 K between hot and cold stream was set in this component. The recovered CH_4 was compressed to 10 bar, dried and injected into the local gas grid, whereas the carbon dioxide was dried and sent to the syngas generator (Table 1).

The two columns required the definition of the loading capacity, the number of stages as well as the insertion of the reaction mechanism to simulate the CO_2 capture process. The loading, i.e., the mole ratio of CO_2 over the mole of amine, was set to 0.24, similarly to the works of Raynal et al. [29] and Li et al. [30]: this value was used to evaluate the lean solvent composition after CO_2 separation. The columns were designed to reduce the thermal needs at the stripper reboiler and to capture 98% of CO_2 entering the system with the biogas flow. Both columns presented 14 stages, with well-mixed flow both in the liquid and vapour phases. Moreover, the stripper presented a kettle reboiler at the bottom stage and a condenser at the top one, with a distillate-to-feed flow ratio of 0.04. Specific components information is listed in section Appendix A.
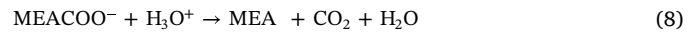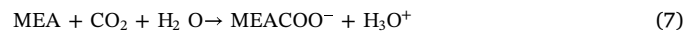
The solvent considered in this study was a mixture of 30 wt-% MEA and 70 wt-% water. The solvent selection was related to its high selectivity towards CO_2, together with its widespread industrial applications despite corrosion and volatility issues. Furthermore, even though MEA-based CO_2 separation is highly energy-intensive, proper thermal integration allows reducing such needs. A carbamate formation mechanism was considered to simulate the process of carbon capture with specific kinetic steps applied as the one proposed by Moioli et al. [31]. Lastly, for this section, the Electrolyte-NRTL (Non-Random Two Liquid) and the Soave-Redlich-Kwong (SRK) state equations described the thermodynamics of the Vapour-Liquid-Equilibrium for the liquid and vapour phase, respectively.

Table 1
Characteristic of the biogas and solvent fed to the CO_2 separation unit.

Biogas Inlet		Composition	[%mol]
Flow rate [m³/hr]	1680	CO_2	0.34
T [K]	298	CH_4	0.65
p [bar]	1	N_2	0.01
Lean Solvent		Composition	[%mol]
Flow rate [kg/s]	6.50	MEA	0.11
T [K]	313	H_2O	0.864
p [bar]	1.07	CO_2	0.026

$$2H_2O \leftrightarrow H_3O^+ + OH^- \tag{1}$$

$$CO_2 + 2H_2O \leftrightarrow HCO_3^- + H_3O^+ \tag{2}$$

$$HCO_3^- + H_2O \leftrightarrow CO_3^{2-} + H_3O^+ \tag{3}$$

$$MEAH^+ + H_2O \leftrightarrow MEA + HCO_3^- \tag{4}$$

$$MEACOO^- + H_2O \leftrightarrow MEA + HCO_3^- \tag{5}$$

$$\ln(K_i) = A_i + B_i/T + C_i\ln(T) + D_iT^{(*)} \tag{6}$$

$$MEA + CO_2 + H_2O \rightarrow MEACOO^- + H_3O^+ \tag{7}$$

$$MEACOO^- + H_3O^+ \rightarrow MEA + CO_2 + H_2O \tag{8}$$

$$CO_2 + OH^- \rightarrow HCO_3^- \tag{9}$$

$$HCO_3^- \rightarrow CO_2 + OH^- \tag{10}$$

$$k_i = A_i\exp(-Eact_i/RT_i)^{(*)} \tag{11}$$

(*) Kinetic coefficients values are available in Appendix A.

2.3. Syngas generation

In this study, a reverse water gas shift reactor and a solid oxide electrolysis stack operating in co-electrolysis mode were selected as possible ways to generate a synthesis gas.

2.3.1. Reverse water gas shift reactor
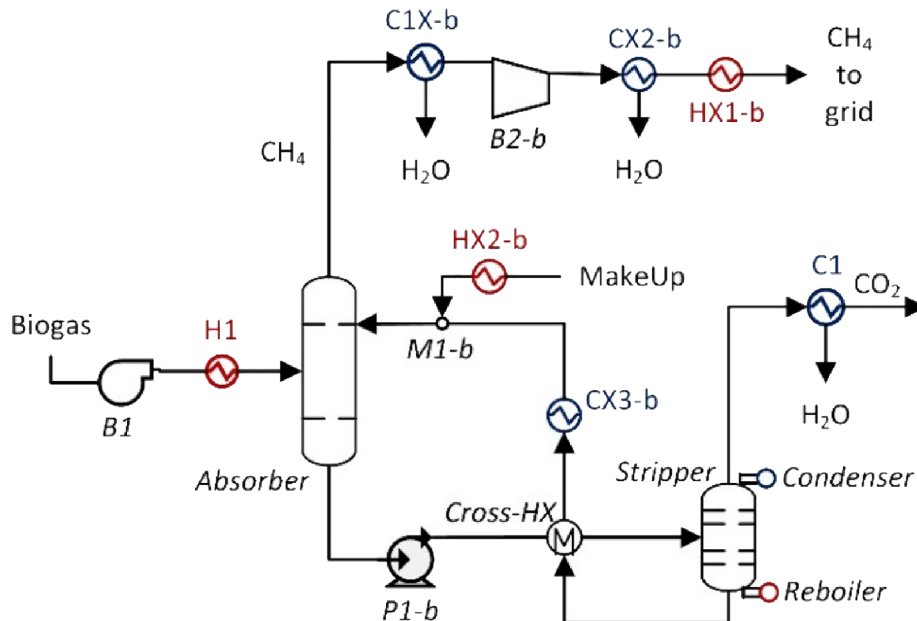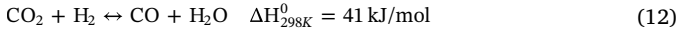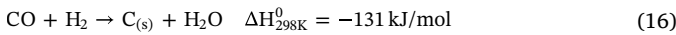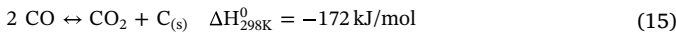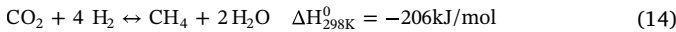The captured carbon dioxide was catalytically converted into

Fig. 2. Biogas upgrading unit schematics.

carbon monoxide inside the RWGS reactor according to:

$$CO_2 + H_2 \leftrightarrow CO + H_2O \quad \Delta H^0_{298K} = 41 \, kJ/mol \quad (12)$$

As demonstrated by Vidal Vazquez et al. [32], the RWGS can reach equilibrium conditions with the proper catalyst selection and the correct reactor size (i.e. catalyst loading, reactor length and diameter). As such, the RWGS reactor employed in this analysis was modelled at equilibrium conditions, minimizing the Gibbs free energy, and loaded with a Ni/Al$_2$O$_3$ catalyst. It operated at 1073 K and ambient pressure, with an inlet gas flow preheated up to 833 K. At equilibrium conditions, also side reactions of methanation and carbon deposition through the Boudouard reaction were taken into account [32]:

$$CO + 3\,H_2 \leftrightarrow CH_4 + H_2O \quad \Delta H^0_{298K} = -165 kJ/mol \quad (13)$$

$$CO_2 + 4\,H_2 \leftrightarrow CH_4 + 2\,H_2O \quad \Delta H^0_{298K} = -206 kJ/mol \quad (14)$$

$$2\,CO \leftrightarrow CO_2 + C_{(s)} \quad \Delta H^0_{298K} = -172 \, kJ/mol \quad (15)$$

$$CO + H_2 \rightarrow C_{(s)} + H_2O \quad \Delta H^0_{298K} = -131 \, kJ/mol \quad (16)$$
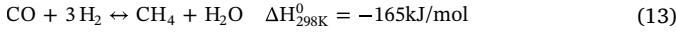
Recirculation of the Fischer-Tropsch off-gas to the RWGS reactor inlet was studied, too. Therefore, the equilibrium model considered also the side reactions of hydrocarbons decomposition and steam reforming of low molecular weight compounds produced during the Fischer-Tropsch reaction entering the RWGS reactor [33]:
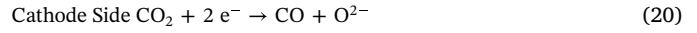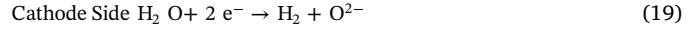
$$C_nH_m \leftrightarrow n\,C + (m/2)\,H_2 \quad e.\,g. \; \Delta H^0\,_{298K} = 791 \, kJ/mol \, CH_4; \, 5960 \, kJ$$
$$/mol\,C_8H_{18} \quad (17)$$

$$C_nH_m + n H_2\,O \leftrightarrow n\,CO + (n+m/2)H_2 \quad e.\,g. \; \Delta H^0_{298K}$$
$$= 206 \, kJ/mol\,CH_4; \, 1277 \, kJ/mol\,C_8H_{18} \quad (18)$$
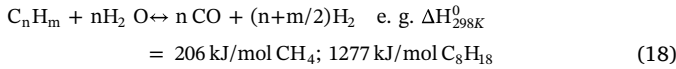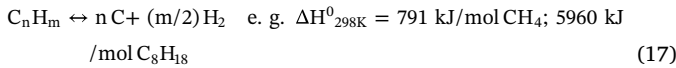
All the captured carbon dioxide from the biogas upgrading unit was exploited and the desired H$_2$/CO molar ratio of 1.9 was obtained by adjusting the inlet water to the electrolysis unit. The alkaline electrolyser delivered H$_2$ at 1 bar and 293 K, with water consumption of 15 L/kg$_{H2}$ and 51 kWh/kg$_{H2}$ [34]. Moreover, steam could be additionally fed at the inlet of the RWGS reactor, if needed to shift the carbon–oxygen-hydrogen equilibrium and avoid solid carbon formation. Lastly, the RWGS applied the SRK equation of state.

2.3.2. Solid oxide electrolysis cell

As one possible alternative, syngas could be produced through a solid oxide electrolysis stack (SOEC) operating under co-electrolysis conditions (i.e., simultaneous splitting of H$_2$O and CO$_2$). The layout of this section is shown in Fig. 3.

The SOEC system operated at 1073 K and atmospheric pressure to match the conditions of the RWGS. Solid oxide cells usually involve as state-of-the-art materials Ni/YSZ cathode, YSZ electrolyte, LSC/CGO anode [35]. The electrochemical reactions for the conversion of CO$_2$-to-CO and H$_2$O-to-H$_2$ followed this presented scheme at cathode and anode sides:

$$Cathode \; Side \; H_2\,O + 2\,e^- \rightarrow H_2 + O^{2-} \quad (19)$$

$$Cathode \; Side \; CO_2 + 2\,e^- \rightarrow CO + O^{2-} \quad (20)$$

$$Anode \; Side \; O^{2-} \rightarrow 0.5\,O_2 + 2\,e^- \quad (21)$$

Chemical reactions taking place at the cathode side were also considered. Due to the simultaneous presence of H$_2$O, CO, CO$_2$ and H$_2$ at the high operating temperature and reactant utilization, Ni also acts as catalyst for the reactions of water gas shift (Eq. (12)) and methane reforming (Eqs. (13) and (14)), which may take place at chemical equilibrium conditions [36]. Also the Boudouard reaction (Eq. (15)) may represent a possible drawback, as it can lead to solid carbon deposition at the Ni cathode matrix, blocking the three-phase points of electrochemical reaction at too low or high reactant utilization [37]. Finally, recirculation of the Fisher-Tropsch off-gases could produce cracking of light hydrocarbons at the stack level (Eqs. (15)–(18)).

In this investigation, the electrochemical conversion of the reactants was modelled using a stoichiometric reactor followed by an O$_2$ separator, as depicted in Fig. 3. The reactions taking place at equilibrium in the fuel electrode were inserted in the model using a reactor at the equilibrium condition after the O$_2$ removal (EQ-2). As demonstrated in other studies, the conversion of CO$_2$-to-CO could be accounted via the WGS reaction in addition to the electrochemical conversion [38]. Finally, in the case of RR values higher than 0%, unconverted CO$_2$, CO, H$_2$ and light hydrocarbons entered the SOEC unit, requiring the simulation of equilibrium reactions also before the O$_2$ separator (EQ-1).

Even in this system configuration with the SOEC module, we assumed to exploit the full flow of CO$_2$ exiting the biogas upgrading unit. The targeted H$_2$/CO molar ratio in the syngas was achieved by variation of the steam flow rate fed to the SOEC. Moreover, a syngas fraction was
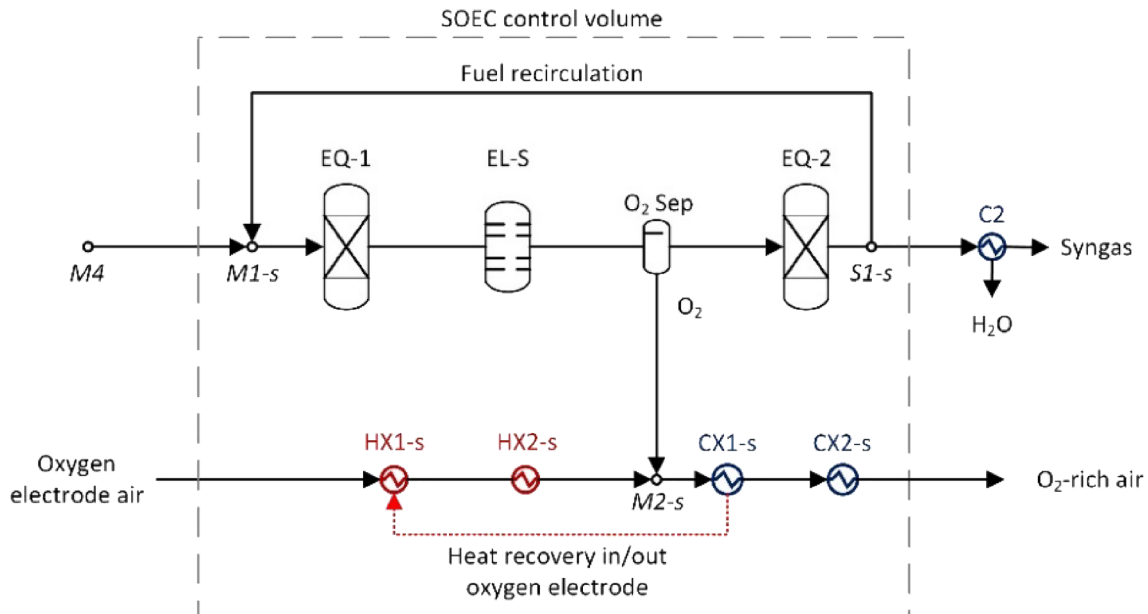

Fig. 3. SOEC stack unit schematics.

recirculated back to the cathode inlet to obtain at least 10 mol-% of H_2 when feeding the SOEC fuel electrode to avoid nickel oxidation [37]. Finally, the effect of FT off-gases recirculation (RR) in the range between 0% and 90% was studied, with special attention to avoid carbon deposition. As such, a reactants utilization (RU) of 75% at stack level was set in the case of ambient pressure operation.

The Faraday's law for co-electrolysis was expressed referring it to the O_2 component to directly include the conversion of both CO_2 and H_2O.

$$\dot{n}_{O_2} = \frac{j\,A_{tot}}{n_{e,tot}F} = \frac{I}{n_{e,tot}F} \tag{22}$$

Being $n_{e,tot}$ the number of total electrons exchanged equal to 4, F the Faraday constant (96485 C/mol). Furthermore, the SOEC was assumed to operate at thermoneutral condition, i.e., the thermal energy produced by the ohmic effect equalled the heat linked to electrochemical and chemical reactions: no external heat was required and the SOEC system was thermally self-sustained [39].

$$V_{OCV} = \frac{\Delta g}{I} \tag{23}$$

$$V_{TN} = \frac{\Delta h}{I} \tag{24}$$

$$j_{TN} = \frac{V_{TN} - V_{OCV}}{ASR} \tag{25}$$

$$A_{tot} = \frac{I}{j_{TN}} \tag{26}$$

The Area-Specific Resistance (ASR) accounting for all the internal losses was set equal to 0.25 Ωcm^2 at ambient pressure, and 0.2 Ωcm^2 at high-pressure conditions [40,41]. Once the thermoneutral operations were ensured, the total electric power to be fed to the SOEC stack could be evaluated.

$$W_{el} = V_{TN}I \tag{27}$$

The reactant utilization referred to the mole flow rate of reactants exiting the stack unit with respect to the feeding, accounting for both electrochemical conversion and for reactions at equilibrium conditions. The fractional conversion of electrochemical reactions was iteratively adjusted in the model to reach the targeted value.
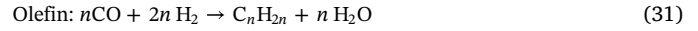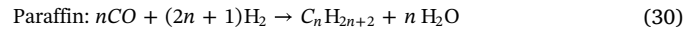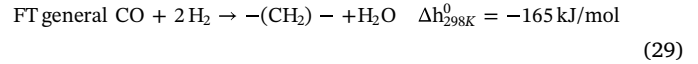
$$RU = \frac{\dot{n}_{react_{in}} - \dot{n}_{react_{out}}}{\dot{n}_{react_{in}}} \tag{28}$$

Lastly, the SRK equation of state was used for modelling this component. Involved compounds are present as vapour phase only.

2.4. Fischer-Tropsch synthesis unit

The Fischer-Tropsch reactor was modelled as a multitubular fixed-bed reactor, operating at 501 K and 25 bar [42]. The operating pressure was reached via a 3-compressors block with intercooling. The involved catalyst was a Co-based one with alumina support, suitable for long-chain hydrocarbon synthesis (Co-Pt/γ-Al$_2$O$_3$) [27]. The reactor was designed as one-through configuration, where no recirculation to its inlet was considered.

In the general FT synthesis theory, the two main products are n-paraffins and α-olefins, with possible formation of aromatic compounds and alcohols. Moreover, the products leaving the reactor follow a modification of the Anderson-Flory-Shultz (AFS) distribution, where a higher methane formation and a lower ethane formation with respect to the ASF distribution are observed. Lastly, the FT product distribution has an exponential behaviour up to carbon number C_{15-20}, after which a linear distribution of the products could be expected [43]. The FT reaction follows the scheme:

FT general $CO + 2\,H_2 \rightarrow -(CH_2)- + H_2O \quad \Delta h^0_{298K} = -165\,kJ/mol$ (29)

Paraffin: $nCO + (2n+1)H_2 \rightarrow C_nH_{2n+2} + n\,H_2O$ (30)

Olefin: $nCO + 2n\,H_2 \rightarrow C_nH_{2n} + n\,H_2O$ (31)

In this study, only paraffins and olefins were considered relevant products, based on previous experimental results on the selected catalyst where negligible amounts of side FT compounds were detected [27]. Moreover, the reactants conversion and the generation of each product were modelled using a rate-based approach. The used kinetic model allowed describing the synthesis of each FT hydrocarbon, defining the product rates based on the syngas partial pressure, temperature and probability growth of the compounds, and to account for the ASF deviations. The detailed derivation of the kinetic model employed in this analysis established on experimental results on a Co-based FT catalyst can be found in [27]. Here we present only the final formulation of the product rates.

$$R_{CH_4} = k_{6M}\alpha_1\sqrt{(K_0 P_{H_2})}\,P_{H_2}\,[vac]^* \tag{32}$$

$$R_{C_2H_4} = k_{7E}e^{2c}\alpha_1\alpha_2\sqrt{(K_0 P_{H_2})}\,[vac]^* \tag{33}$$

$$R_{C_nH_{2n+2}} = k_6\alpha_1\alpha_2\prod_{n=3}^{n}\alpha_n\sqrt{(K_0 P_{H_2})}\,P_{H_2}\,[vac]; \quad \text{for } n \geq 2^* \tag{34}$$

$$R_{C_nH_{2n}} = k_7 e^{nc}\alpha_1\alpha_2\prod_{n=3}^{n}\alpha_n\sqrt{(K_0 P_{H_2})}\,[vac]; \quad \text{for } n \geq 3^* \tag{35}$$

* The definition $\alpha_{i\text{-th}}$ and [vac] can be found in Appendix B.

The kinetic model is based on the carbide mechanism for the description of the FT reaction, and both reactants and products rates follow a LHHW formulation. K_{ith} and k_{ith} are the rate and equilibrium constants, respectively; α_{ith} the probability growth at each carbon number; p the partial pressure of hydrogen and carbon monoxide. A plug flow reactor working at isothermal conditions was selected, with the application of an external kinetic subroutine for rates definition up to C_{80} for paraffins and C_{40} for olefins (the detailed information about the kinetic external subroutine implementation can be found in the supplementary material file).

From the molar balance of carbon monoxide between the reactor inlet and outlet, it was possible to evaluate the CO conversion. This was set in all cases to a fixed per-pass value of $X_{CO} = 75\%$ under no FT off-gases recirculation condition [44]. This value was selected to suppress both the water gas shift reaction over cobalt (relevant at $X_{CO} > 80\%$), as well as to reduce the formation of methane and light hydrocarbons, which were unwanted products compared to targeted long-chain hydrocarbons [45]. Finally, 35% catalyst bed porosity was assumed in the reactor model.

$$X_{CO} = \frac{\dot{n}_{CO_{inFT}} - \dot{n}_{CO_{outFT}}}{\dot{n}_{CO_{inFT}}} \tag{36}$$

The thermodynamic model applied in the FT unit was the RKS equation of state, with Boston-Mathias alpha value modification (SRK-BM), accounting for hydrocarbon and petrochemical problems for non-polar mixtures, such as in the FT-synthesis. Petrochemical compounds with carbon number higher than C_{30} were inserted inside the AspenPLUS™ environment from external databases.

2.5. FT products distillation

The separation of the FT products consisted of three consecutive steps. A first three-phase separator operating at constant ambient temperature divided water from the gas and liquid FT fractions. The liquid compounds underwent a first distillation process separating naphtha from middle distillates, wax and residual gas fractions. A second distillation tower provided the separation of light waxes from

heavy waxes. Both distillation towers were modelled with reference to the boiling temperature of each fraction cut operating at ambient pressure. To evaluate the final tower size, a first estimation with the Winn-Underwood-Gilliland method allowed finding the theoretical minimum number of stages and minimum reflux ratio at ambient pressure required to separate each fraction [46]. Consequently, the distillation towers were substituted and modelled with a more rigorous PetroFrac component in AspenPLUS™, which accounted for the presence of kettle reboilers at the bottom stage, a condenser at the top stage and side strippers. The first distillation tower had a total number of 54 stages, with a reflux ratio of 1.8. It had a side stripper of 16 stages, with draw at stage 18 and overhead return at stage 12 of the main column. It presented a preheating up to 523 K at the inlet of the tower. The second distillation column was composed of 58 stages and a reflux ratio of 1.8. The tower separated the light wax fraction from the heavy fraction. The FT products entering the second distillation tower were preheated to 728 K [46,47]. Hydrocarbons cuts temperatures selected for each of the fractions are presented in Table 2.

Off-gases leaving the first distillation tower were mixed with the off-gases coming from the 3-phase separator. The fraction not recirculated back to the inlet of the syngas generator was burnt. The burner operated at atmospheric pressure, with air-excess conditions. The airflow needed for the combustion was iteratively changed to reach a combustion temperature of 1273 K [48].

2.6. Energy integration and system efficiency evaluation

Energy integration was carried out to minimize the external heat requirement. Pinch analysis methodology was applied to all thermal streams of each plant configuration, matching cold with hot fluids (the first being those streams that increase their temperature, the latter the ones in need of refrigeration). Both hot and cold composite curves were built considering a minimum difference of temperature at the pinch point of 288 K. Finally, plant efficiencies and key performance indicators were selected. In the biogas upgrading section, the specific reboiler heat duty GJ/ton$_{CO2}$, the CO_2 capture rate and stream purity and the section efficiency (η_{Biogas}) were considered.

$$\eta_{Biogas} = \frac{\dot{n}_{CH_4}LHV_{CH_4}}{W_{el_{biogas}} + Q_{net_{biogas}} + \dot{n}_{biogas}LHV_{biogas}} \quad (37)$$

Additionally, the efficiency of the syngas generation and FT reaction were evaluated:

$$\eta_{Syngas+FTR} = \frac{\sum_{FTsyncrude} \dot{n}_i LHV_i}{W_{el_{Syngas+FTR}} + Q_{net_{Syngas+FTR}}} \quad (38)$$

Finally, the global system efficiency (η_{Glob}) and the overall carbon reduction potential were estimated:

$$\eta_{Glob} = \frac{\dot{n}_{CH_4}LHV_{CH_4} + \sum_{FTsyncrude} \dot{n}_i LHV_i}{W_{el_{net}} + Q_{net} + \dot{n}_{biogas}LHV_{biogas}} \quad (39)$$

$$CRP = \frac{\dot{n}_{CO_2 Biogas} - \dot{n}_{CO_2 Exhaust}}{\dot{n}_{CO_2 Biogas}} \quad (40)$$

The total system efficiency η_{Glob} considered the whole process, from the CO_2 separation in the biogas-upgrading unit to the ventilation towards the atmosphere of the exhaust gases. To account for the energy content of the FT products in [kJ/mol], a correlation for paraffins and olefins derived by Stempien et al. [49] was used:

$$LHV_{Par.} = 608.44n + 213.31 \quad (41)$$

$$LHV_{Olef.} = 604.93n + 113.83 \quad (42)$$

3. Results

Both syngas generation options (SOEC and RWGS) account for two different solutions, without FT off-gas recirculation (0% RR) and 90% of the FT off-gas recirculation (90% RR). Moreover, the hypothesis considered for the comparison of the models are the following:

- Use of all the captured CO_2 from the biogas upgrading unit: 1 ton/hr;
- Fix FT reactor size obtained at 75% CO conversion and 0% RR;
- Avoid carbon deposition at the syngas generation unit;
- Maximization of the CRP;
- Maximization of the middle distillate and wax fraction throughput;
- Minimization of the energy demand.

3.1. CO_2 separation unit

The biogas upgrading section is common to each different plant configuration. This section provides a capture rate of 98% of the total CO_2 injected into the plant and 99.9% recovery of the CH_4. The CO_2 purity is about 98%, while the separated stream has a methane purity of 98.5%. Both values are in line with similar applications of biogas upgrading with chemical absorption solutions [50–52]. Moreover, the specification of the CH_4 stream makes it suitable for a possible injection in the gas grid, having a Wobbe Index of 50.6 MJ/Sm^3 and a high heating value of 37.9 MJ/Sm^3 [53]. On the other hand, the great system separation performance results in high specific heat duty for the solvent regeneration at the stripper reboiler stage of 4.75 GJ$_{th}$/ton$_{CO2}$, in good agreement with literature values for MEA-based plants (3.5–5 GJ/ton$_{CO2}$) [54,55]. Such value would result in high heat consumption for a biogas upgrading system. However, when combined with a power-to-liquid technology with proper energy integration, such external thermal needs can be reduced or avoided. Exact outlet composition and specifics of the main components are presented in Table 3.

The results listed in Table 3 show that the purity of the CO_2 stream is only counteracted by the presence of inert N_2 gas, while the amount of CH_4 leaving the biogas upgrading unit from the carbon dioxide side is negligible. This becomes very important when coupling such a device with a Fischer-Tropsch reactor, where the presence of CH_4 may inhibit the formation of high molecular weight hydrocarbons. Moreover, a reintegration of the MEA and water looping in the system is required. This loss is connected to phenomena of entrainment, volatilization and degradation in the columns and heat exchangers mainly [30,56]. Lastly, the cross heat exchanger allows having an internal heat transfer on 860 kW from the stripping column to the outlet flow of absorption column (Fig. 2).

3.2. FT product synthesis

In all cases, a reference configuration can be selected at H_2/CO molar ratio of 1.9, with a recirculation rate of the Fischer-Tropsch off-gases at 0%.

3.2.1. Baseline configuration: 0% RR

Carbon dioxide is sent from the biogas upgrading unit to the syngas generator. Water is fed to the alkaline electrolyser and delivered in the

Table 2
Different product classes obtained after the distillation of the FT products.

Fraction	Carbon Number	Boiling Temperature [K]
Gas	C_1-C_4	313
Naphtha	C_4-C_{11}	396
Middle Distillate	C_{11}-C_{20}	498
Light Waxes	C_{20}-C_{35}	656
Heavy Waxes	C_{35}-C_{70+}	793

Table 3

Composition of the separated CH_4 stream and CO_2 stream and final parameters of the components obtained after the simulation.

CO₂ stream				
Mole flow rate	18.8	[mol/s]	Composition	[% mol]
		CO_2	97.96	
		CH_4	0.02	
		H_2O	2.03	
		N_2	0.0	
CO_2 separation efficiency	$[CO_{2out}/CO_{2in}]$	98.4%		
CH₄ stream	**[mol/s]**	**Composition**	**[% mol]**	
Mole flow rate	12.5	CO_2	0.02	
		CH_4	98.47	
		H_2O	0.06	
		N_2	1.51	
Wobbe Index	[MJ/Sm³]	50.56		
HHV	[MJ/Sm³]	37.88		
CH_4 separation efficiency	$[CH_{4out}/CH_{4in}]$	99.9%		
Components				
Stripper reboiler	[kW_th]	1313.2		
Stripper condenser	[kW_th]	−227.1		
Stripper specific heat duty	[GJ_th/ton_CO2]	4.75		
Cross Heat Exchanger duty	[kW_th]	860.6		
Biogas blower	[kW_el]	7.44		
Circulation pump	[kW_el]	0.69		
CH_4 Compressor	[kW_el]	103.3		
Make-up flow	[mol/s]	17.87	MEA	2.5
			H2O	97.5

form of H_2 in case A, or to the SOEC unit after vaporization as steam in case B. Table 4 provides a summary of the most relevant information of the mass balances of the reference configuration at 0% RR.

Considering the synthesis of useful FT products, the configuration with the solid oxide electrolyser allows reaching a greater production. This is related to the chemical and technical limitations associated with the RWGS reactor, which reaches a maximum carbon dioxide conversion lower than the one obtained with the SOEC (63% and 75% for case A and case B, respectively). This directly impacts the synthesis of hydrocarbons in the Fischer-Tropsch reactor, given the lower CO availability for further processing. CO_2 might act as inert gas under the FT reaction, providing no useful reactant for the synthesis of the hydrocarbons [57]. Consequently, a lower amount of air to the combustor is required for case A. It is worth to notice that the reached fractional conversion of CO_2 in the reactor is confirmed by other studies that report RWGS applications [24,58]. Moreover, the RU of the SOEC unit could be additionally increased to 80–85%, determining a further rise in the CO_2 consumption rate. However, the value has been kept to a maximum of 75% to avoid possible solid carbon deposits. Concerning the global CRP, case B reaches a higher value than case A, given the higher conversion contribution of the syngas unit.

In terms of thermal and electrical energy consumptions and processes efficiencies, the results are listed in Table 5. The thermal needs of the system with SOEC stack are higher. Firstly, the generation of steam is highly energy-intensive. Secondly, the higher amount of FT products needs more heat to process the separation in the distillation towers (case A 39.2 kW_th, case B 44.9 kW_th). On the contrary, the electricity consumed by the alkaline electrolyser is higher than the one absorbed by the SOEC, impacting more on the global efficiency η_{Glob} described by Eq. (48). Moreover, in both cases, the most energivorous process is related to the separation of CO_2 inside the stripper of the biogas upgrading unit. The electrical consumption of the different sections is also provided. In the case of the biogas upgrading unit only, the most energy demanding element is the compressor of the biomethane for grid injection (103.3 kW_el). This corresponds to 93% of the electricity required

by the biogas upgrading section, and 32.4% of the total plant electricity in case A and 29.5% in case B. Lastly, for both cases A and B the 3-compressors unit needed before the FT reactor accounts for about 4% of the total electrical needs. In this component, the higher electrical needs of case B is again related to the marginally different gas composition entering the FT reactor, affecting the compression (Table 6 provides the composition of the gas entering the FT reactor).

Considering the technical specifics of the main components, the Fischer-Tropsch reactor results in 19.25 m³ and 18.06 m³ in case A and B, respectively. Moreover, case A has an RWGS reactor that requires 309.4 kW to operate at isothermal conditions. Lastly, the SOEC consumes 3.6 MW_el at thermoneutral condition, corresponding to a voltage of 1.35 V (OCV at 0.96 V) and a current density of 0.58 A/cm², leading to a total required area of 455.7 m².

3.2.2. Upgrading of the systems: 90% RR

The recirculation of the FT off-gases enables increasing the throughput of useful products and providing a rise in the total conversion of CO_2. A value of 90% recirculation rate has been selected as a trade-off between the increase in useful FT material, conversion of carbon dioxide and rise in the energy demand due to the higher amount of FT products that have to be processed by the distillation columns. In addition, higher RR could result in accumulation of inert gases in the system lines [59].

In both the configurations, the recirculation is exponentially beneficial for the synthesis of the targeted waxes, middle distillates and naphtha, whereas it reduces the generation of methane and light hydrocarbons thanks to their cracking inside the syngas units. Specifically, case A provides a slightly higher amount of FT syncrude than case B. Possibly, the high conversion of CO_2 in the SOEC results in a high amount of CO processed by the FT reactor and transformed into gas fraction. Therefore, the iterative recirculation of the off-gases of case B determines a consequently higher amount of material fed to the burner and not recycled compared to case A (Table 7).

In case A, the endothermicity of the RWGS reactor requires 1.1 MW_th to operate at isothermal conditions. With a similar demand rise with respect to the 0% RR case, the SOEC needs the supply of 5.3 MWel at thermoneutral conditions, reaching 1.50 V (OCV at 0.94 V), a thermoneutral current of 0.84 A/cm² and a total area of 418.8 m².

In terms of global process efficiency, each configuration presents a similar value to the cases at 0% recirculation rate, with slightly lower values at 90% RR. This is due to a rise in the energy demand (thermal and electrical) that counterbalances the beneficial increase of useful FT products. Specifically, a great supply of energy is required by the RWGS reactor to operate at 1073 K, by the SOEC steam generator and by the distillation towers processing the FT products. As expected from the mass balance, in the latter case of separation columns, a slightly higher amount of energy is required by case A (98.2 kW_th against 96.7 kW_th). On the other hand, the recirculation increases both the local and global

Table 4

Case A and Case B 0% RR mass balance.

Mass Flow Rate [kg/h]	Case A	Case B
Biogas Inlet	1745	1745
Captured CO_2	1002.8	1002.8
Biogas Up. CH_4	728	728
H_2O for electrolysis	1297.4	774.1
Naphtha C_{5-11}	26.1	31.4
Middle distillate C_{11-20}	31.3	37.0
Light wax C_{20-35}	20.9	24.9
Heavy wax C_{35+}	9.9	11.8
Steam to avoid C-deposition	0.0	0.0
Total condensed water	809.0	761.7
Combustion air	5022.1	5812.1
Exhaust gas	5549.0	6266.3
CRP	27.5%	34.2%
CO₂ Conversion at Syngas Section	*63.0%*	*75.0%*

Table 5

Energy consumptions and process efficiencies at 0% RR. [a] Complete information of the thermal balance is provided in Appendix C. [b] SOEC working at the thermoneutral condition: no heat exchange with the environment is required.

Thermal balance [kW$_{th}$][a]	Case A	Case B
Total Heating Needs	2432.9	2659.5
Biogas Section	*1346.6*	*1346.6*
Steam Generation	*–*	*755.9*
RWGS/SOEC	*309.4*	*_[b]*
FT Products Distillation	*39.3*	*44.9*
Others	*737.6*	*512.1*
Cooling Needs (Towards the environment)	−4678.2	−5165.8
Fischer-Tropsch Reactor [kJ/mol$_{CO}$]	−167.4	−168.7
Fischer-Tropsch Reactor Volume [m³]	*19.25*	*18.06*
Electrical balance [kW$_{el}$]		
Biogas Upgrading Section	111.5	111.5
Syngas + FT Section	207.8	236.1
B2	*1.7*	*–*
B3	*61.9*	*67.4*
B4	*69.3*	*84.2*
B5	*69.5*	*84.5*
B-Cdep	*–*	*–*
Electrolysis	4341.1	3569.4
Energy content [kW]		
Biogas Feed	9868.5	9868.5
FT Products	−1079.3	−1285.5
Biogas Up. CH$_4$	−9867.3	−9867.3
Process Efficiencies		
η$_{Biogas}$	87.2%	87.2%
η$_{Syngas+FT}$	19.2%	25.2%
η$_{Glob}$	64.5%	67.8%

Table 6

Gas molar composition at the outlet of the RWGS (Case A) and SOEC (Case B).

[% mol]	Case A 0% RR	Case B 0% RR	Case A 90% RR	Case B 90% RR
CO	22.5%	25.8%	30.1%	28.9%
H$_2$	42.7%	49.1%	57.3%	54.9%
H$_2$O	22.9%	16.5%	8.0%	10.5%
CH$_4$	0.0%	0.1%	0.4%	0.3%
CO$_2$	11.8%	8.5%	4.2%	5.4%

conversion of carbon dioxide: a greater material flow is processed inside the RWGS or SOC systems. The effect of recirculation is depicted in Fig. 4: the recirculation of the FT off-gases could be considered beneficial.

3.2.3. Carbon deposition

Solid carbon formation can lead to catalyst deactivation, reducing the performance of the entire process. It has been experimentally detected both on RWGS and SOEC technologies [60,61]. To avoid carbon deposition, different solutions can be applied. With RWGS reactors, a lower reactant conversion or an increase in the steam-to-carbon ratio can be carried out [60,62]. Similarly, coke deposition onto the SOC stack layers can be avoided with a variation of the reactants utilization, addition of steam or modification of the electrode with dopants deposition [36,63]. Moreover, with an increase of the recirculation rate, solid carbon formation could be stronger due to the higher presence of carbon compounds dragged into the syngas unit generators with the recirculated stream, with a higher contribution of Eqs. (15)–(18). However, thermodynamic calculations show that no solid carbon deposits at the RWGS nor SOEC systems at the given conditions. Fig. 5 provides the evolution of the thermodynamic equilibrium of cases A

Table 7

Mass and energy balance of case A and case B at 90% RR. [a] SOEC working at the thermoneutral condition: no heat exchange with the environment is required. [b] Complete information of the thermal balance is provided in Appendix C.

Mass Balance [kg/h]	Case A	Case B
Biogas Inlet	1745	1745
Captured CO$_2$	1002.8	1002.8
Biogas Up. CH$_4$	728	728
H$_2$O for electrolysis	2002.0	1274.9
Steam to avoid C-deposition	0.0	0.0
Total Condensed Water	1103.1	1185.8
Combustion Air	2349.0	2398.2
Exhaust Gas	2458.7	2522.1
Naphtha C$_{5-11}$	79.9	77.3
Middle distillate C$_{11-20}$	93.7	93.4
Light wax C$_{20-35}$	61.1	59.3
Heavy wax C$_{35+}$	24.9	23.7
Thermal Balance [kW$_{th}$][a]		
Heating Need	3342.1	3639.1
Biogas Section	*1346.6*	*1346.6*
Steam Generation	*–*	*1245.1*
RWGS/SOEC	*1089.7*	*_[b]*
FT Products Distillation	*98.2*	*96.7*
Recirculation Heating	*233.3*	*394.3*
Others	*574.3*	*556.4*
Cooling Need (Towards to environment)	−5734.6	−6254.3
Fischer-Tropsch Reactor [kJ/mol$_{CO}$]	−169.8	−169.3
Fischer-Tropsch Reactor Volume [m³]	*19.25*	*18.06*
Electric Balance [kW$_{el}$]		
Biogas Upgrading Section	111.5	111.5
Syngas + FT Section	540.9	613.9
B2	*2.6*	*–*
B3	*168.7*	*174.9*
B4	*188.8*	*218.8*
B5	*179.6*	*219.6*
B-Cdep	*–*	*–*
Electrolysis	6698.7	5280.9
Energy content [kW]		
Biogas Feed	9868.5	9868.5
FT Products	−3168.6	−3110.5
Biogas Up. CH$_4$	−9867.3	−9867.3
Process Efficiencies		
CRP	81.1%	79.6%
CO$_2$ Conversion at Syngas Section	*97.3%*	*97.3%*
η$_{Biogas}$	87.2%	87.2%
η$_{Syngas+FT}$	34.4%	38.2%
η$_{Glob}$	63.4%	66.5%

and B at increasing recirculation rates at the outlet of the RWGS and SOEC units. As both cases at ambient pressure do not reach any solid carbon formation conditions, no additional steam is required by the RWGS reactor nor a reduced RU in the SOC stack. Lastly, no carbon formation has been detected experimentally nor with modelling in the Fisher-Tropsch reactor.

3.3. Energy integration

The optimal energy integration of the thermal streams can improve system performance by reducing the external thermal need. Given the higher throughput of products that can be obtained in the 90% RR configurations, the energy integration results are presented for these cases only, in this work.

Table 8 lists the main results derived from the energy integration of the streams, while the composite curves of the two cases are shown in Fig. 6. In terms of hot composite curves, cases A and B have a similar shape. The majority of the thermal power at a high temperature can be recovered from the cooling of the exhaust gases vented towards the
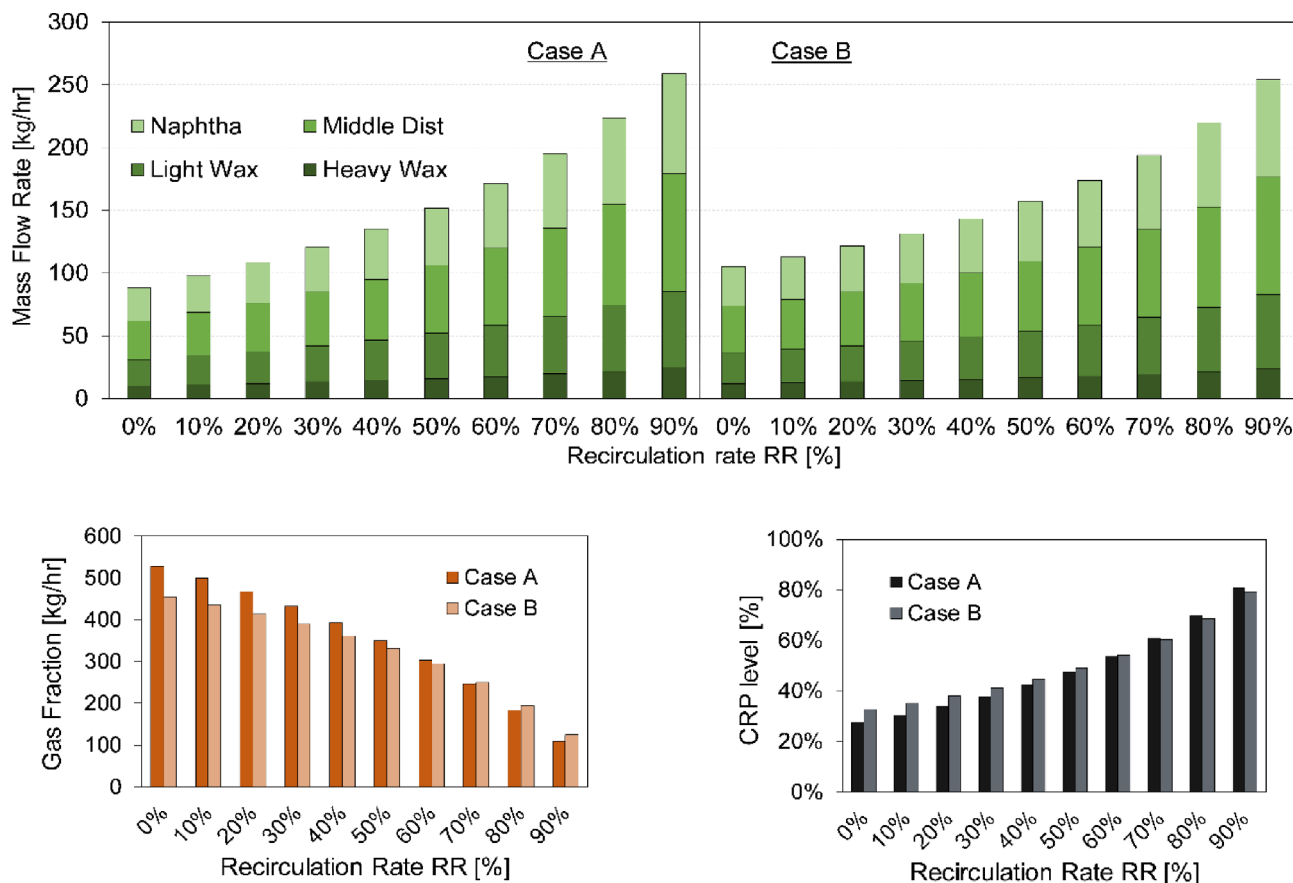
Fig. 4. Effect of the increased in the recirculation rate: top) FT products; bottom-left) Gas fraction; bottom-right) carbon reduction potential.

environment: case A 747 kW$_{th}$, case B 760 kW$_{th}$. Moreover, both configurations present a plateau at 501 K, corresponding to the heat released by the exothermic activity of the Fischer-Tropsch reactor, accounting for 25% and 23% of the total available heat of the systems for case A and B, respectively. Considering the cold composite curves, two plateaus can be identified for every configuration. The first is related to the heat required by the reboiler of the biogas upgrading unit at 388 K. A second one can be identified at low temperature for the SOEC stack

for the vaporization of the water entering the stack themselves, and at high temperature for the RWGS to keep the reactor at the operating temperature. As such, the presence of high temperature heat demand related to the RWGS determines an increased external energy consumption in case A, with a lowering of the global systems efficiency with respect to case B. As summarized in Table 8, the final thermal needs of the RWGS system correspond to 0.9 MW$_{th}$. This could be supplied by high-temperature electric heaters. In the case of the SOEC
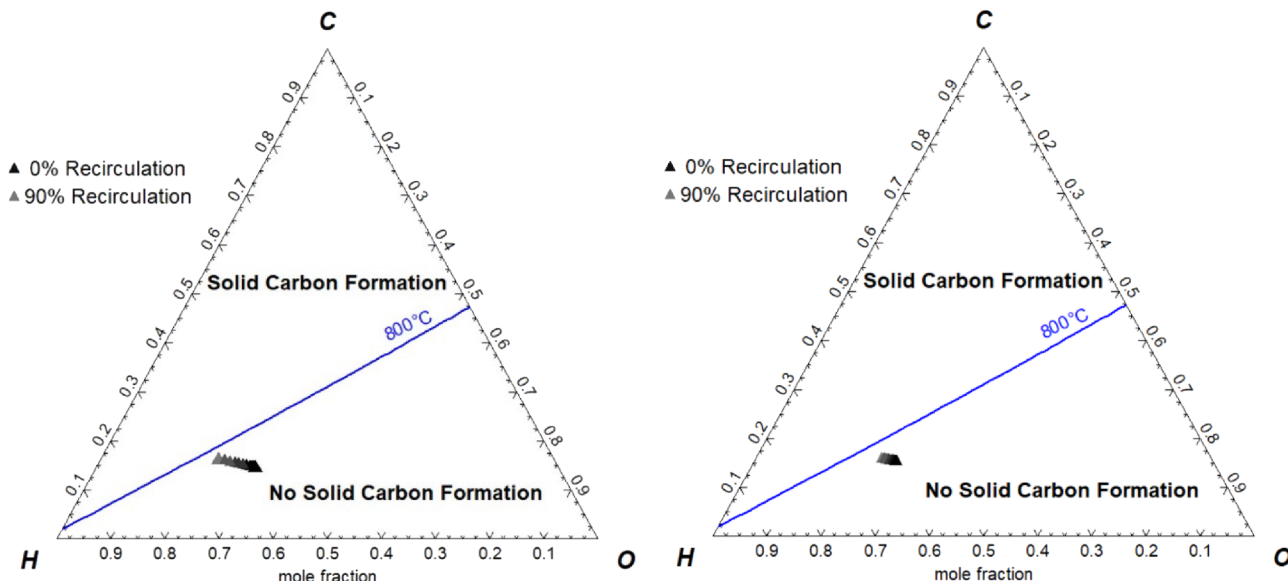

Fig. 5. Ternary diagrams of solid carbon formation at increasing value of RR: left) Case A, outlet of the RWGS reactor; right) Case B, outlet of the SOE electrolyser.

Table 8
Effect of the energy integration of the total energy consumption and plant efficiencies at 90% RR.

Pinch Point Temperature [K]	Case A		Case B	
	1080.7		1265.7	
	Before Integration	*After Integration*	*Before Integration*	*After Integration*
Total heating Demand [kW$_{th}$]	3340.2	1000.5	3639.1	0.0
Total cooling demand [kW$_{th}$]	−5734.6	−3358.1	−6254.3	−2615.3
η_{Glob}	63.4%	71.5%	66.5%	81.8%

stack, all the thermal needs can be covered with internal system heating generation. Under configuration A, heat recovery from internal flows corresponds to 70.1% of the total heat required by the system upon integration, whereas configuration B reaches 100% recovery, given the lower demands of the SOEC against the RWGS at high temperature. For instance, referring to the most impacting heat sources and sinks, above the pinch point of configuration A 145 kW can be transferred from the exhausts cooling to the RWGS reactor, to partially sustain its endothermicity activity. Below the pinch point, the same heat source transfers 233 kW to the recirculated FT gas fraction. The syngas cooling for water condensation can supply 460 kW to preheat the mixture entering the RWGS reactor and the FT products entering the first distillation columns and to the reboiler of the column. Similarly, 80 kW are transferred to the preheater of the FT material entering the second distillation column and to the same column reboiler. The exothermicity of the FT can be exploited in the biogas upgrading unit stripper (1313 kW) and to preheat both the biogas and the make-up flow entering this unit. Similar considerations can be given in configuration B, where all the heat exchanges take place below the pinch point temperature. The cooling of the exhaust gases can heat the recirculated gas fraction, the SOEC sweep air and preheat the water up to zero vapour fraction (541 kW). The cooling of the syngas can preheat the mixture entering the SOEC, sustain the reboiler requirements for the distillation towers and provide thermal power for the biogas stripper (716 kW). The exothermicity of the FT can sustain the vaporization of the water for the electrochemical reaction and part of the heat required by the biogas stripper (1229 kW). Finally, for all the cases, excess heat is available at low temperature. In this study, this heat has been considered as a waste, however, it can be employed for steam generation or low-temperature heating of local users.

4. Discussion

The overall highest plant efficiency corresponds to 81.8%. This value can be reached with optimal energy integration for case B at 90%

RR. The second-highest efficiency is reached at similar condition, but employing the integrated RWGS in place of the SOEC stack (71.5%). On the one hand, the very high values can be related to the energy content of the recovered methane in the biogas upgrading unit. On the other hand, the ideal integration of the stream sensibly reduces the energy needs coming from the outside. With respect to similar studies where CO_2 capture is inserted in the plant process, Vidal et al. [24] achieved a system efficiency as high as 47% when coupling an FT reactor with an RWGS with direct air capture. With biomass gasification, Leibbrandt et al. [64] reached a value of 51%. Monaco et al. [65] calculated efficiency of 65.9% and 62% with CO_2 recovered from biomass upgrade and biogas upgrade, respectively. As such, the present model represents a highly efficient solution to combine a CO_2 capture system with FT synthetic chemicals production.

Samavati et al. [66] and Cinti et al. [19] obtained 85% and 57.2% plant efficiency, operating with a solution SOEC + FT. Selvatico et al. [21] of 43.7% with an RWGS + FT solution. In this study, considering only the section of CO_2 upgrade to FT products, the highest $\eta_{Syngas+FTR}$ efficiencies correspond to 38.3% and 34.4% for a recirculation rate of 90% for case B and A, respectively. However, by optimally integrating only the section after the CO_2 separation, the efficiency $\eta_{Syngas+FTR}$ would reach a value of 38.7% for case A and of 52.7% for case B, making this plant configuration without CO_2 capture still competitive with other studies from the literature.

4.1. H₂/CO molar ratio effect

A variation of the ratio of hydrogen-to-carbon monoxide at the inlet of the Fischer-Tropsch reactor can affect the synthesis of FT products. The Fischer-Tropsch process requires a feed gas with a molar ratio of H_2/CO around 2.0 to account for the stoichiometry of the reaction taking place over the catalytic bed [67]. A rise in the H_2/CO ratio reduces the synthesis of high molecular weight hydrocarbons for the stoichiometry of the Fischer-Tropsch synthesis, by means of lower probability growth at Eqs. ((31)–(38)). This results in higher selectivity
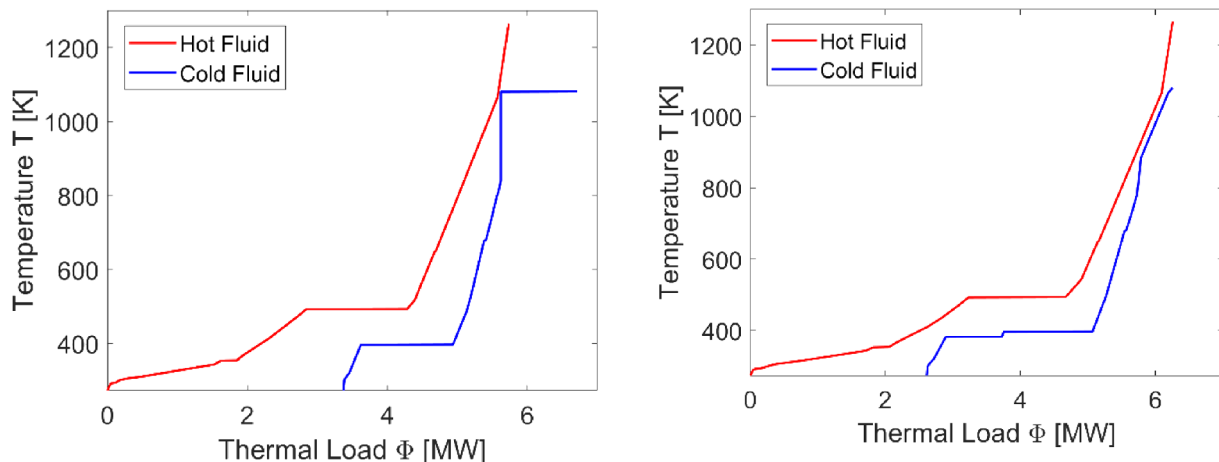

Fig. 6. Composite curves derived by the pinch analysis at 90% RR: left) Case A; right) Case B.

of lighter hydrocarbons and lowers CRP values by means of more material fed to the burner. Contrariwise, having lower H_2/CO values provides α_{ith} towards unity, and thus increases the yield of wax production. However, the heat duty of the distillation towers would consequently rise. Moreover, this solution shifts the equilibrium of the FT reaction towards the reactants and reduces the total reaction rates and CO conversion. For instance, reducing the H_2/CO to 1.6 would result in X_{CO} of 67% in case A and of 66.5% in case B. Similarly, Campanario et al. [48] found that reducing the H_2/CO from 2.3 to 1.7 increases the production of FT material but increases also the energy consumption. Lillebø et al. [68] experimentally demonstrated how reducing the H_2/CO ration reduces the CO conversion (Fig. 7).

4.2. Effect of pressure variation

Given the need for high-pressure operation of the Fischer-Tropsch reactor, a solution with RWGS and SOEC at high pressure can be evaluated. Mass and energy balances are summarized in Table 9.

With reference to the synthesis of the useful FT products, it is possible to note how the high-pressure configurations allow reaching a lower yield of production with respect to their low-pressure counterparts, regardless of the recirculation rate. This is related to the nature of the reactions involved in the syngas generator units, which further influences the performance of the Fischer-Tropsch reactor. For both the RWGS reactor and the SOEC stack, Eq. (12) is equimolar, meaning that a change in pressure does not influence the equilibrium of the reaction. However, the reactions of methanation (eq. (13)–(14)) are shifted towards the products at high pressure by means of the Le Chatelier principle [69]. This behaviour is depicted in Fig. 8, where the effect of pressure is presented. For both configurations, the methane yield of

production rises with an increment of the pressure up to 25 bar, determining a reduction of the CO available at the outlet of the reactors with respect to the ambient pressure case. However, this is an unwanted product in power-to-liquid applications with FT reactors, counteracting the synthesis of long-chain hydrocarbons. Furthermore, a decrease in the value of CO_2 conversion can be observed at increasing pressures, possibly due to more favourable conditions for Eq. (13). Lastly, the drop in the CO_2 conversion for SOEC is further enhanced by the need for reducing the reactants utilization value to avoid solid carbon formation at pressures higher than 15 bar.

Concerning the energy balance, pressure increase leads to a reduction in the plants' thermal needs when operating at 0% RR. On the contrary, at 90% RR, high-pressure configurations present a higher material content at the recirculated stream that needs to be heated up to the operating temperature, thus increasing the thermal requirement of the plants with respect to the atmospheric pressure solutions. Finally, the configurations operating at ambient pressure provides higher plant efficiency (global and limited to syngas + FT sections) given the same performance of the biogas upgrading unit: a lower amount of FT products at the system outlet results in a lower energy content for the configurations at high pressure, i.e., lower plant efficiency. Furthermore, the SOC system requires the compression of a high amount of air to ensure the electrochemical conversion of the reactants, making it the least performing configuration on both the $\eta_{Syngas+FT}$ and η_{gl}. However, the compression of the reactants before the RWGS or SOEC requires less electrical energy than the case of compression before the FT reactor. Finally, pressure increase implies a stronger control to avoid coking. In the case of the RWGS, this is avoided by adding steam when operating at 90% RR (no C-deposition is detected at 0% RR and 25 bar). In the case of the SOEC, the RU needs to be reduced from 75%
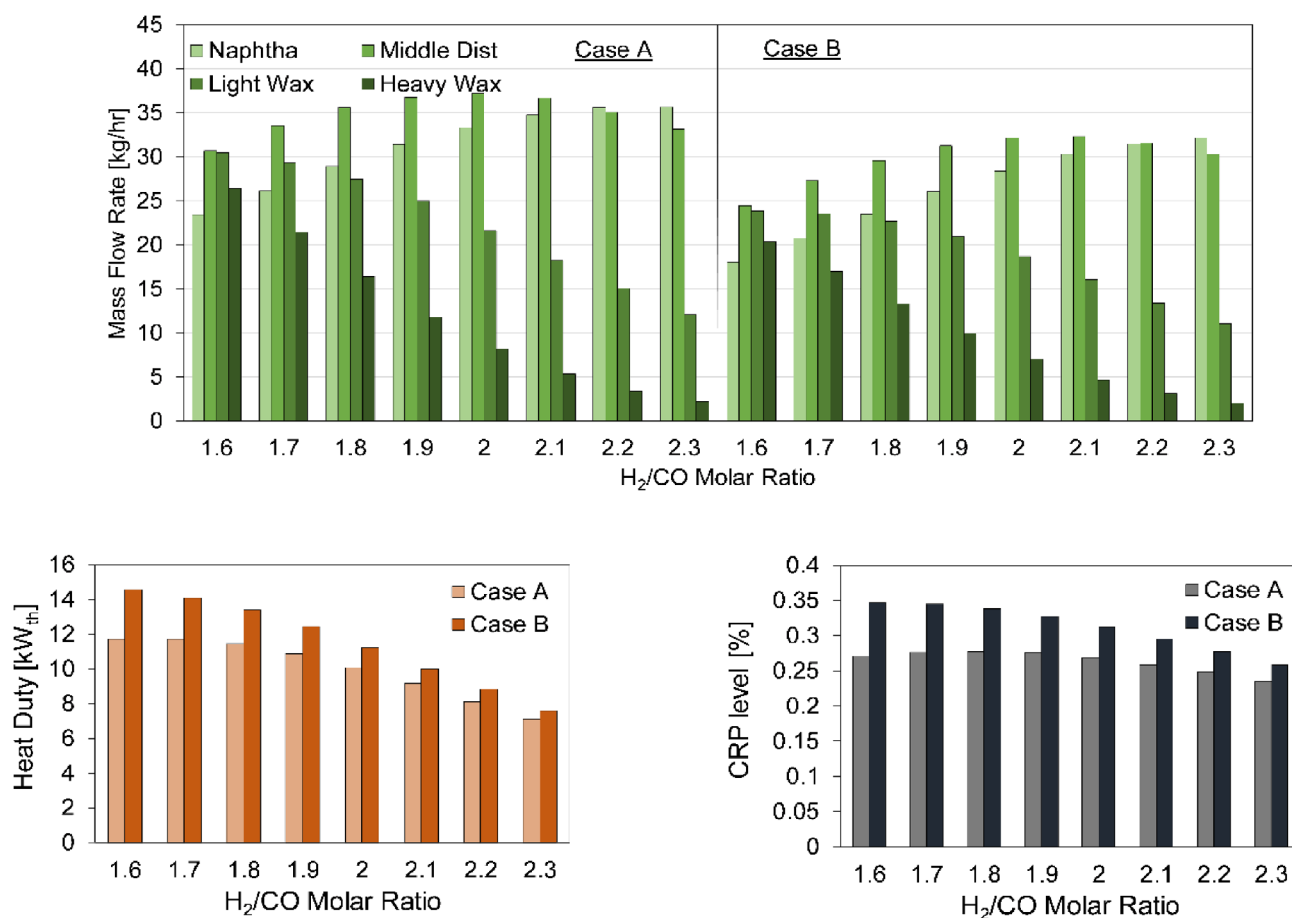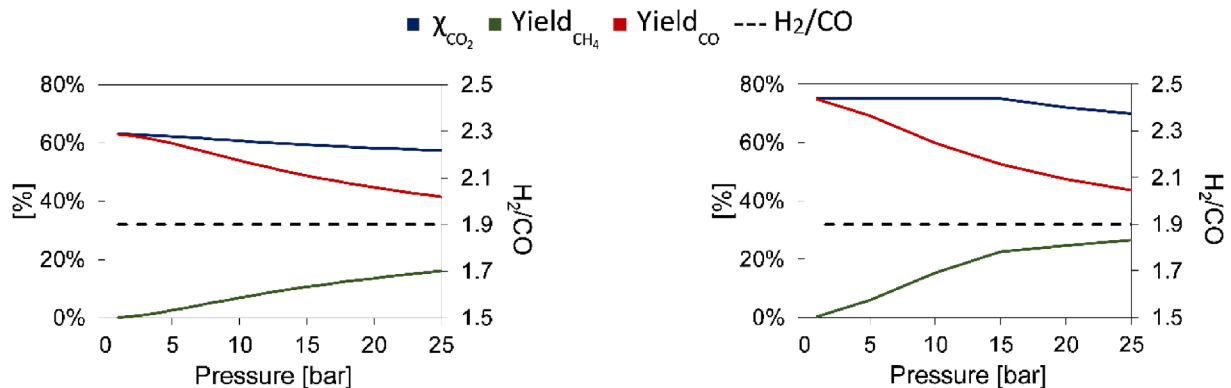

Fig. 7. Effect of H_2/CO molar ratio in the syngas over: top) FT products; bottom-left) Heat duty for FT products separation; bottom-right) CRP.

Table 9

Mass and energy balance with syngas generators operating at high pressure (25 bar) at 0% and 90% RR.

Mass Balance [kg/h]	Case A 0% RR		Case B 0% RR		Case A 90% RR		Case B 90% RR	
Biogas Inlet	1745		1745		1745		1745	
Captured CO_2	1002.8		1002.8		1002.8		1002.8	
Biogas Up. CH_4	728		728		728		728	
H_2O for electrolysis	1312.6		786.4		1858.1		2125.4	
Steam to avoid C-deposition	0.0		0.0		840.5		0.0	
Total Condensed Water	786.5		707.9		1851.8		2045.3	
Combustion Air	6539.4		7697.0		4594.2		4043.9	
Exhaust Gas	7126.5		9060.6		4859.9		4325.5	
Naphtha C_{5-11}	15.2		17.1		52.8		58.2	
Middle distillate C_{11-20}	18.7		17.4		72.5		67.6	
Light wax C_{20-35}	12.1		12.3		43.1		43.2	
Heavy wax C_{35+}	5.6		5.7		16.2		16.2	
Fischer-Tropsch Reactor [kJ/mol$_{CO}$]	−167.96		−167.93		−169.07		−169.09	
Fischer-Tropsch Volume [m³]		*19.12*		*18.98*		*19.12*		*18.98*
Thermal Balance [kW$_{th}$]								
Heating Need	2096.3		3005.2		5075.9		5593.9	
Biogas Section		*1346.6*		*1346.6*		*1346.6*		*1346.6*
Steam Generation		*–*		*759.7*		*836.3*		*2050.9*
RWGS/SOEC		*61.2*		*–*		*1296.5*		*–*
FT Products Distillation		*22.9*		*23.1*		*71.6*		*75.9*
Recirculation Heating		*–*		*–*		*617.4*		*938.7*
Others		*665.5*		*875.8*		*907.4*		*1181.7*
Cooling Needs	4842.1		5333.5		7591.1		8042.8	
Electric Balance [kW$_{el}$]								
Biogas Upgrading Section	111.5		111.5		111.5		111.5	
Syngas + FT Section	93.7		958.8		110.9		1125.5	
B1-HP		*69.3*		*69.3*		*69.3*		*69.3*
B2		*1.7*		*–*		*2.4*		*–*
B2-HP		*22.7*		*–*		*32.2*		*–*
B3-HP		*–*		*–*		*0.6*		*0.3*
B4-HP		*–*		*1.8*		*–*		*4.8*
B-Cdep		*–*		*–*		*2.3*		*–*
Air comp. SOEC		*–*		*888*		*–*		*1051.4*
Electrolysis	4391.9		3400.5		6217.1		4742.9	
Energy content [kW]								
Biogas Feed	9868.5		9868.5		9868.5		9868.5	
FT Products	−631.9		−640.5		−2257.9		−2264.1	
Biogas Up. CH_4	−9867.3		−9867.3		−9867.3		−9867.3	
Process Efficiencies								
CRP	16.1%		18.1%		58.5%		58.6%	
CO_2 Conversion at Syngas Section		*60.5%*		*70.0%*		*86.9%*		*84.6%*
η_{Biogas}	87.2%		87.2%		87.2%		87.2%	
$\eta_{Syngas+FT}$	12.1%		10.2%		22. %		22.2%	
η_{Glob}	63.4%		60.6%		56.7%		56.6%	

Fig. 8. Pressure effect on the syngas generators over CO_2 conversion, CH_4 yield, CO yield and H_2/CO molar ratio: left) Case A; right) Case B.
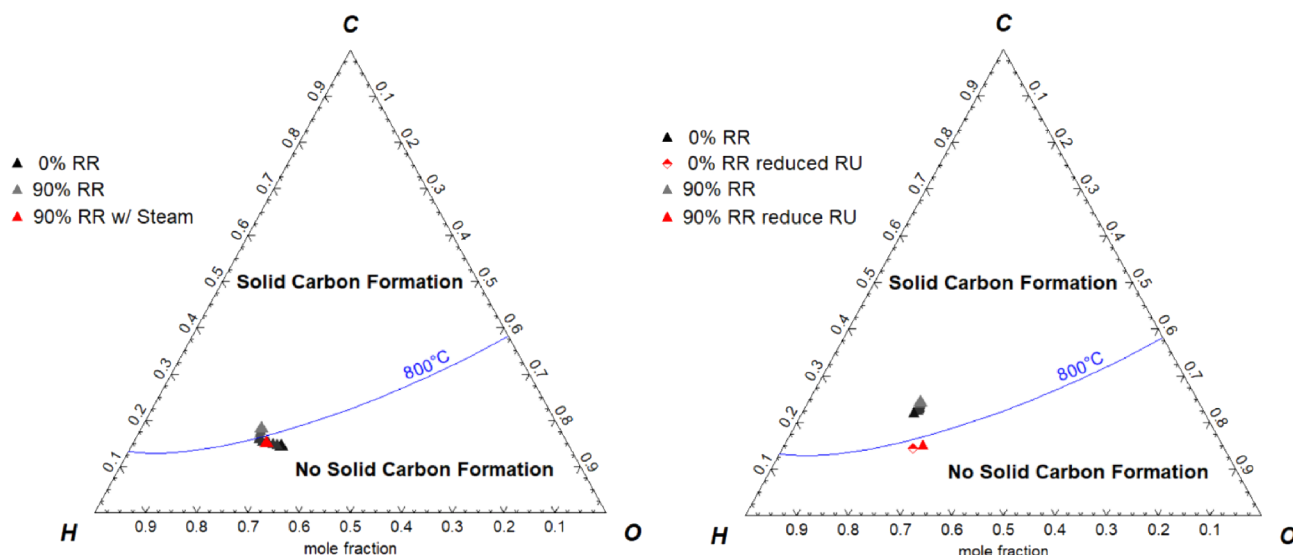
Fig. 9. Ternary diagrams of solid carbon formation at increasing value of RR with syngas generators working at 25 bar: left) Case A, outlet of the RWGS reactor; right) Case B, outlet of the SOE electrolyser.

Table 10
Energy integration effect on the total energy consumption and plant efficiencies at 90% RR at high pressure operation of the syngas generators.

Pinch Point Temperature [K]	Case A		Case B	
	1080.7		493.9	
	Before Integration	*After Integration*	*Before Integration*	*After Integration*
Total Heating Need [kW$_{th}$]	5075.9	1000.5	5593.9	153.0
Total Cooling Need [kW$_{th}$]	7591.1	3535.0	8042.8	6749.1
η_{Glob}	56.7%	70.1%	56.6%	75.8%

to 70% at 0% RR and to 40% if recycling 90% of the FT off-gases (Figs. 9 and 10).

4.3. Technology readiness level

Schmidt et al. [70] identified the technology readiness levels (TRL) of several devices for carbon capture and utilization for P2L. Consequently, the TRL of different P2L routes with Fischer-Tropsch reactor has been included. They could determine that the overall TRL of a P2L route is downgraded to the lowest TRL of the production chain. Both the biogas upgrading with MEA and the Fischer-Tropsch reactor are considered highly developed systems, with TRL 9. On the contrary, the RWGS and SOEC devices present lower TRLs. For instance, the RWGS presents a TRL of 6, while the SOEC has been estimated at TRL ranging from 3 to 5 whether it accounts for CO_2 electrolysis or not [71].

In our study, a solution employing a solid oxide electrolyser under co-electrolysis at ambient pressure seems to be the best fit to produce FT products from industrial CO_2 in terms of plant efficiency. This solution can replace the RWGS reactor and the low-temperature electrolyser into one single component and allow for high plant efficiency thanks to thermoneutral operation. However, this device is not yet available at a commercial level for the required capacities, whereas the RWGS is a proven technology. As a matter of fact, a solution as case A could be considered at TRL 6, while a solution as case B would fall to TRL much lower, making its deployment more expensive. On the contrary, a solution with the RWGS provides slightly lower η_{Gl} but allows for higher FT products synthesis when operating at 90% RR. As such, a

further economic assessment will be carried out in order to identify the most proficient plant configuration from an energy and economic point of view.

4.4. On the catalyst selection

In the present analysis, a Co-based catalyst was employed to synthetize long-chain hydrocarbons. Even though Co is more expensive than Fe (the other largely employed catalyst in FTS), it shows better activity and enhanced selectivity towards linear C_{5+} FTS compounds [18]. In order to make PtL routes more appealing, not only optimal process modelling is required, but also studying the synthesis of performance-enhanced catalysts becomes a key aspect to target specific products. Rytter et al. [72] suggested that large pores on catalyst supports would influence positively the selectivity towards C_{5+}. Moreover, the presence of structural promoters such as K, Ce, Cs, Mn, Pt can improve the catalysts activity, shift the selectivity and reduce their degradation. For instance, Yang et al. [45] showed how K-promotion would decrease the activity of their Fischer-Tropsch Co catalyst. However, Mn-promotion would reduce the production of methane in favour of longer chain products. Gavrilovic et al. [73] determined optimal Pt effect on different-sized Co particles. However, the cost associated to the involved rare metal con negatively affect both installation, and operation costs [74]. Also innovative and recent catalyst synthesis techniques like the atomic layer deposition (ALD) are proving to be an attractive solution to design resilient and precise catalysts, with enhanced performance and desired morphology. For instance, O'Neill et al. [74] demonstrated how ALD can used to effectively control the active sites distribution and size, and influence the catalyst selectivity. Eskelinen et al. [75] provided experimental data showing the effect of ALD Pt-promotion on Co-catalyst and variation in light products selectivity under FTS against traditionally impregnated catalysts. However, if the ALD seems to be a very attracting technological solution, its cost for catalyst production is sensibly higher than traditional techniques due to a low deposition rate [76]. As such, PtL systems require precise analysis and trade-off between installation and operation costs, the first ones related to technologies and materials employed, the second ones linked, among other factors, to optimal system integration before their implementation.

5. Conclusions

The present study provides a complete analysis of two systems for the recovery of waste industrial carbon dioxide from a biogas upgrading plant, and its upgrade to Fischer-Tropsch synthetic hydrocarbons. Case A uses an RWGS reactor for the generation of syngas, case B a SOEC operating under co-electrolysis conditions. The Fischer-Tropsch reactor is modelled using a kinetic model that describes the formation of each FT product based on experimental results.

The analysis shows that:

- The biogas upgrading unit can separate 98% of CO_2 content in the biogas stream at the expenses of high energy consumption (4.75 GJ_{th}/ton_{CO2});
- When operating under a baseline condition of 0% RR, the solution with the RWGS converts a lower amount of CO_2 to useful products due to an intrinsic limitation of the technology at equilibrium condition. Moreover, case B reaches a slightly higher η_{Glob} of 67.8% against 64.5% of case A thanks to the higher energy content of the FT products;
- Applying a recirculation of the FT off-gases to a rate as high as 90% allows increasing exponentially the production of synthetic hydrocarbons, the deployment CO_2 and the overall plant efficiency. Similarly, the configuration with the SOEC stack provides an efficiency of 66.7% against 63.4% of case A. On the contrary, the recirculation allows reaching a higher production of syncrude when applying an RWGS reactor;
- Regardless of the technology, increasing the operating pressure of the syngas generator to 25 bar (thus matching the pressure of the FT reactor) reduces the production of useful syncrude. However, overall plant efficiency is only a few percentage points lower with respect to the ambient pressure cases. Moreover, while RWGS reactors operating at high pressure are commercially available, SOEC systems under co-electrolysis are only present at the laboratory and demonstration scale. As such, a pressurized case B is not a

recommended option, whereas pressurized case A would need proper design and economic evaluation.

- Energy integration of the plant streams can drastically reduce the energy input required from the outside, diminishing also the impact that a high energy-intensive process like the biogas upgrade can have. Case A at 90% RR thermal needs reduce from 3.3 MW_{th} to 0.9 MW_{th}, while in case B the reduction is from 3.5 MW_{th} to 0 MW_{th}.
- Given the TRL of the different technologies, fast and effective commercialization of this specific process concept would need the implementation of a P2L with an RWGS reactor. An economic assessment including a real heat exchangers network is required to identify the most proficient plant configuration.

CRediT authorship contribution statement

Marco Marchese: Methodology, Formal analysis, Investigation, Software, Data curation, Writing - original draft, Visualization. **Emanuele Giglio:** Supervision, Formal analysis, Investigation, Resources, Writing - review & editing. **Massimo Santarelli:** Supervision, Writing - review & editing. **Andrea Lanzini:** Supervision, Project administration, Writing - review & editing.

Declaration of Competing Interest

The authors declare that they have no known competing financial interests or personal relationships that could have appeared to influence the work reported in this paper.

Acknowledgements

Appendix A

Table A1
Specifications of the biogas section components.

Preheater outlet	313 K	Solvent Cooler outlet	313 K
Absorber	Rate-based 1.07 bar (Δp 0.5 bar) 14 stages 1 m section diameter Mixed Flow model Interfacial area factor 1.2 Reaction condition factor 0.9 Film discretization ratio 5	Stripper	Rate-based 1.6 bar (Δp 0.5 bar) 14 stages (with condenser and reboiler) 1 m section diameter Mixed Flow model Interfacial area factor 1.2 Reaction condition factor 0.9 Film discretization ratio 5 Distillate to feed ratio 0.05

Table A2
Reaction coefficients for the chemical reactions of the biogas upgrading unit Eq. (1)–(5) [31].

Reaction	Coefficients			
	A	B	C	D
(1)	132.89	−13445.9	−22.47	0
(2)	231.46	−12092.1	−36.78	0
(3)	216.05	−12431.7	−35.48	0
(4)	−3.038	−7008.36	0	−0.0031
(5)	−0.52	−2545.53	0	0

Table A3
Reaction coefficients for the chemical reactions of the biogas upgrading unit Eqs. (7)–(10) [77].

Reaction	A_j	E_{act} [cal/mol]
(7)	9.77e + 10	9850
(8)	2.18e + 18	14138.4
(9)	4.32e + 13	13,249
(10)	2.38e + 17	29,451

Appendix B

$$\alpha_1 = \frac{k_1 P_{CO}}{k_1 P_{CO} + k_{6M} P_{H2}} \tag{43}$$

$$\alpha_2 = \frac{k_1 P_{CO}}{k_1 P_{CO} + k_6 P_{H2} + k_{7E} e^{c2}} \tag{44}$$

$$\alpha_N = \frac{k_1 P_{CO}}{k_1 P_{CO} + k_6 P_{H2} + k_7 e^{cn}} n \geq 3 \tag{45}$$

[vac]

$$= 1/\left\{ 1 + \sqrt{(K_0 P_{H_2})} * \left(1 + \alpha_1 + \alpha_1 \alpha_2 + \sum_{j=3}^{n_c} \prod_{n=3}^{j} \alpha_n \right) + \left(\alpha_1 + \alpha_1 \alpha_2 + \sum_{j=3}^{n_c} \prod_{n=3}^{j} \alpha_n \sum_{j=3}^{n_c} \prod_{n=3}^{j} \alpha_n \right) \left[\frac{1}{K_4} + \frac{1}{\sqrt{(K_0 P_{H_2})} K_3 K_4} + \frac{P_{H2O}}{(K_0 P_{H_2})^{(1.5)} K_2 K_3 K_4 K_5} \right] \right.$$

$$\left. + \frac{1}{K_5} \frac{P_{H2O}}{\sqrt{(K_0 P_{H_2})}} \right\} \tag{46}$$

Appendix C

Table C1
Information about the components employed in this study.

Component	Description	Technical information
Biogas upgrading section		
B1	Biogas blower	Target pressure 1.12 bar
Absorber	Absorber of the biogas upgrading section	14 stages, 1.12 bar, Δp 0.05 bar, 313 K
Stripper	Stripper of the biogas upgrading section, with condenser top stage and reboiler bottom stage	14 stages, 1.6 bar, Δp 0.1 bar, partial-vapour condenser (362.3 K), kettle reboiler (388.8 K)
P1-b	Circulation pump	Target pressure 1.6 bar, η_{el} 0.95
B2-b	Methane compressor	Target pressure 10 bar; η_{is} 0.85, η_{mech} 0.95
H1	Biogas heater	Target temperature 313 K
HX1-b	CH_4 heater	Target temperature 293 K
Hx2-B	Make-Up flow heater	Target temperature 313 K
C1	CO_2 cooler	Target temperature 288 K
CX1-b	CH_4 cooler	Target temperature 283 K
CX2-b	CH_4 cooler after compression	Target temperature 558 K
CX3-b	Looping cooler pre absorber	Target temperature 313 K
Cross-HX	Heat exchanger for heat recovery at the biogas upgrading unit	ΔT 15 K
M1-b	Mixer for make-up flow injection	
Case A and B at reference condition		
Alk. electrolyser	Conversion of water to hydrogen in case A, accounting for auxiliaries consumptions	15 L/kg_{H2} consumed, 50 kW_{el}/kg_{H2}
RWGS reactor	Isothermal reactor working at equilibrium condition for the generation of syngas	Operating at 1073 K, 1–25 bar, Δp 0.1 bar
FT reactor	Isothermal reactor working at rate-based conditions for the generation of FT products	Operating at 501 K, 25 bar, Δp 0.1 bar
SOEC stack	Conversion of CO2 and H2O to syngas in case B	Operating at 1073 K, 1–25 bar, Δp 0.1 bar
3-phase separator	Separation of water from the gas and liquid FT fractions at constant temperature	Operating at 298 K
Col1	Petrochemical fractionations of the FT products, with one side stripper: gas, naphtha, middle distillate, wax	54 stages, 1 bar, reflux ratio 1.8, partial-vapour-liquid condenser (301 K), kettle reboiler (670 K); Stripper (16 stage) draw stage 18, overhead return stage 12, top stage condenser 456 K
Col2	Petrochemical fractionation of the FT wax fraction into light and heavy waxes	58 stages, 1 bar, reflux ratio 1.8, total condenser (656 K), kettle reboiler (793 K)
Furnace	Combustion of the FT off-gases and unconverted compounds	Operating at 1273 K, ambient pressure

Table C1 (*continued*)

Component	Description	Technical information
V1	Lamination valve	Target pressure 1 bar
V2	Lamination valve	Target pressure 1 bar
V3	Lamination valve	Target pressure 1 bar
V4	Lamination valve	Target pressure 1 bar
B2	Pump for water entering in the alkaline electrolyser, only for case A (consumption accounted in the alkaline electrolysers block)	Target pressure 15 bar
B3	Intercooling compressor, only with ambient air operation of the syngas units	Pressure ratio 2.924, from ambient pressure; η_{is} 0.85, η_{mech} 0.95
B4	Intercooling compressor, only with ambient air operation of the syngas units	Pressure ratio 2.924; η_{is} 0.85, η_{mech} 0.95
B5	Intercooling compressor, only with ambient air operation of the syngas units	Pressure ratio 2.924; η_{is} 0.85, η_{mech} 0.95
C2	Condenser at the outlet of the syngas generator units	Target temperature 293 K
C3	Intercooling cooler, only with ambient air operation of the syngas units	Target temperature 373 K
C4	Intercooling cooler, only with ambient air operation of the syngas units	Target temperature 373 K
C5	Intercooling cooler, only with ambient air operation of the syngas units	Target temperature 501 K
C6	Cooling simulation at the entrance of the 3-phase separator	Target temperature 298 K
C7	Cooling the exhaust gases leaving the furnace	Target temperature 323 K
C8	Cooling the naphtha FT fraction	Target temperature 298 K
C9	Cooling the middle distillate FT fraction	Target temperature 298 K
C10	Cooling the light waxes FT fraction	Target temperature 298 K
C11	Cooling the heavy waxes FT fraction	Target temperature 298 K
H2	Preheating of the gas mixture at the inlet of the syngas generator units	Target temperature 1073 K
H3	Preheating of the FT liquid entering the first distillation column	Target temperature 523 K
H4	Preheating of the wax fraction entering the second distillation column	Target temperature 728 K
H5	Preheating of air entering the furnace	Target temperature 473 K
H6	Preheating of the FT off-gases recirculated to the syngas generation unit	Target temperature 1073 K
H7	Heating for steam generation entering the SOEC, only for case B	Target temperature 1073 K
H-Cdep	Heater for steam generation needed to avoid carbon deposition, only for case A	Target temperature 1073 K
B-Cdep	Pump for water needed to avoid carbon deposition, only for case A	Target pressure 1–25 bar, η_{el} 0.95
M1	Mixer of the syngas generators reactants	
M2	Mixer of FT off-gases	
M3	Mixer of FT off-gases and air at the furnace inlet	
S1	Splitter for recirculation of the FT off-gases	
SOEC Section		
Electr. Reactor	Stoichiometric reactor accounting for electrochemical conversion of CO_2 and H_2O, accounting for pressure drop	Operating at 1073 K, 1–25 bar, Δp 0.1 bar
Ch. Eq. (1)	Equilibrium reactions taking place inside the SOEC	Operating at 1073 K
Ch. Eq. (2)	Equilibrium reactions taking place inside the SOEC	Operating at 1073 K
O2 Sep.	Simulator of O_2 generation inside the SOEC	100% recovery of O_2
HX1-s	Preheating of the inlet air at the oxygen electrode with recovery of heat from the outlet of the oxygen electrode	ΔT 15 K with CX1-s
HX2-s	Heater of the air entering the oxygen electrode of the SOEC	Target temperature 1073 K
CX1-s	Cooling of the O2-rich air at the outlet of the oxygen electrode, with heat recovery to the inlet air	ΔT 15 K with HX1-s
M1-s		
M2-s		
S1-s		
Components needed in the case of pressurised syngas generator units		
B1-HP	Compressor for CO_2	Target pressure 25 bar; η_{is} 0.85, η_{mech} 0.95
B2-HP	Compressor for H2, only case A	Target pressure 25 bar; η_{is} 0.85, η_{mech} 0.95
B3-HP	Compressor for recirculation	Target pressure 25 bar; η_{is} 0.85, η_{mech} 0.95
B4-HP	Pump for water, only case B	Target pressure 25 bar, η_{el} 0.95
H1-HP	Heater for syngas entering the FT reactor	Target temperature 501 K

Appendix D. Supplementary data

Supplementary data to this article can be found online at https://doi.org/10.1016/j.ecmx.2020.100041.

References

[1] Jones CR, Olfe-Kräutlein B, Naims H, Armstrong K, Jones CR. The Social acceptance of carbon dioxide utilisation: a review and research agenda. Front Energy Res 2017;5:1–13. https://doi.org/10.3389/fenrg.2017.00011.

[2] Chehade Z, Mansilla C, Lucchese P, Hilliard S, Proost J. Review and analysis of demonstration projects on power-to-X pathways in the world. Int J Hydrogen Energy 2019;44:27637–55. https://doi.org/10.1016/j.ijhydene.2019.08.260.

[3] Cuellar-Franca RM, Azapagic A. Carbon capture, storage and utilisation technologies: a critical analysis and comparison of their life cycle environmental impacts. J CO₂ Util 2014;9:82–102. https://doi.org/10.1016/j.jcou.2014.12.001.

[4] Panahi M, Yasari E, Rafiee A. Multi-objective optimization of a gas-to-liquids (GTL) process with staged Fischer-Tropsch reactor. Energy Convers Manag 2018;163:239–49. https://doi.org/10.1016/j.enconman.2018.02.068.

[5] Ye C, Dang M, Yao C, Chen G, Yuan Q. Process analysis on CO₂ absorption by monoethanolamine solutions in microchannel reactors. Chem Eng J 2013;225:120–7. https://doi.org/10.1016/j.cej.2013.03.053.

[6] Hombach LE, Doré L, Heidgen K, Maas H, Wallington TJ, Walther G. Economic and environmental assessment of current (2015) and future (2030) use of E-fuels in light-duty vehicles in Germany. J Clean Prod 2019;207:153–62. https://doi.org/10.1016/j.jclepro.2018.09.261.

[7] Hanaoka T, Miyazawa T, Shimura K, Hirata S. Jet fuel synthesis from Fischer-Tropsch product under mild hydrocracking conditions using Pt-loaded catalysts. Chem Eng J 2015;263:178–85. https://doi.org/10.1016/j.cej.2014.11.042.

[8] Kiss AA, Pragt JJ, Vos HJ, Bargeman G, de Groot MT. Novel efficient process for methanol synthesis by CO₂ hydrogenation. Chem Eng J 2016;284:260–9. https://doi.org/10.1016/j.cej.2015.08.101.

[9] Salomone F, Giglio E, Ferrero D, Santarelli M, Pirone R, Bensaid S. Techno-economic modelling of a Power-to-Gas system based on SOEC electrolysis and CO₂ methanation in a RES-based electric grid. Chem Eng J 2019;377. https://doi.org/10.1016/j.cej.2018.10.170.

[10] De Klerk A. Can Fischer-Tropsch syncrude be refined to on-specification diesel fuel? Energy Fuel 2009;75:4593–604. https://doi.org/10.1021/ef9005884.

[11] Van der Laan GP, Beenackers AACM. Kinetics and selectivity of the fischer-tropsch synthesis: a literature review. Catal Rev 1999;4940:255–318. https://doi.org/10.1081/CR-100101170.

[12] Rafati M, Wang L, Dayton DC, Schimmel K, Kabadi V, Shahbazi A. Techno-economic analysis of production of Fischer-Tropsch liquids via biomass gasification: the effects of Fischer-Tropsch catalysts and natural gas co-feeding. Energy Convers Manag 2017;133:153–66. https://doi.org/10.1016/j.enconman.2016.11.051.

[13] Kim HH, Mazumder M, Lee M-S, Lee S-J. Effect of blending time on viscosity of rubberized binders with wax additives. Int J Pavement Res Technol 2018;11:465–65. https://doi.org/10.1016/j.IJPRT.2018.03.003.

[14] Mehran MT, Bin Yu S, Lee DY, Hong JE, Lee SB, Park SJ, et al. Production of syngas from H₂O/CO₂ by high-pressure coelectrolysis in tubular solid oxide cells. Appl Energy 2018;212:759–70. https://doi.org/10.1016/j.apenergy.2017.12.078.

[15] Ma R, Xu B, Zhang X. Catalytic partial oxidation (CPOX) of natural gas and renewable hydrocarbons/oxygenated hydrocarbons – a review. Catal Today 2019;338:18–30. https://doi.org/10.1016/j.cattod.2019.06.025.

[16] Ostadi M, Rytter E, Hillestad M. Evaluation of kinetic models for Fischer-Tropsch cobalt catalysts in a plug flow reactor. Chem Eng Res Des 2016;114:236–46. https://doi.org/10.1016/j.cherd.2016.08.026.

[17] Moazami N, Wyszynski ML, Mahmoudi H, Tsolakis A, Zou Z, Panahifar P, et al. Modelling of a fixed bed reactor for Fischer-Tropsch synthesis of simulated N₂-rich syngas over Co/SiO₂: Hydrocarbon production. Fuel 2015;154:140–51. https://doi.org/10.1016/j.fuel.2015.03.049.

[18] dos Santos RG, Alencar AC. Biomass-derived syngas production via gasification process and its catalytic conversion into fuels by Fischer Tropsch synthesis: a review. Int J Hydrogen Energy 2019. https://doi.org/10.1016/j.ijhydene.2019.07.133.

[19] Cinti G, Baldinelli A, Di A, Desideri U. Integration of solid oxide electrolyzer and Fischer-Tropsch: a sustainable pathway for synthetic fuel. Appl Energy 2016;162:308–20. https://doi.org/10.1016/j.apenergy.2015.10.053.

[20] Fazeli H, Panahi M, Rafiee A. Investigating the potential of carbon dioxide utilization in a gas-to-liquids process with iron-based Fischer-Tropsch catalyst. J Nat Gas Sci Eng 2018;52:549–58. https://doi.org/10.1016/j.jngse.2018.02.005.

[21] Selvatico D, Lanzini A, Santarelli M. Low temperature Fischer-Tropsch fuels from syngas: kinetic modeling and process simulation of different plant configurations. Fuel 2016;186:544–60. https://doi.org/10.1016/j.fuel.2016.08.093.

[22] Herz G, Reichelt E, Jahn M. Techno-economic analysis of a co-electrolysis-based synthesis process for the production of hydrocarbons. Appl Energy 2018;215:309–20. https://doi.org/10.1016/j.apenergy.2018.02.007.

[23] Rafiee A, Panahi M, Khalilpour KR. CO₂ utilization through integration of post-combustion carbon capture process with Fischer-Tropsch gas-to-liquid (GTL) processes. J CO₂ Util 2017;18:98–106. https://doi.org/10.1016/j.jcou.2017.01.016.

[24] Vázquez Francisco Vidal, Koponen Joonas, Ruuskanen Vesa, Bajamundi Cyril, Kosonen Antti, Simell Pekka, Ahola Jero, Frilund Christian, Elfving Jere, Reinikainen Matti, Heikkinen Niko, Kauppinen Juho, Piermartini Paolo. Power-to-X technology using renewable electricity and carbon dioxide from ambient air: SOLETAIR proof-of-concept and improved process concept. J CO₂ Util 2018;28:235–46. https://doi.org/10.1016/j.jcou.2018.09.026.

[25] Tagomori IS, Rochedo PRR, Szklo A. Techno-economic and georeferenced analysis of forestry residues-based Fischer-Tropsch diesel with carbon capture in Brazil. Biomass Bioenergy 2019;123:134–48. https://doi.org/10.1016/j.biombioe.2019.02.018.

[26] Comidy LJF, Staples MD, Barrett SRH. Technical, economic, and environmental assessment of liquid fuel production on aircraft carriers. Appl Energy 2019;256:113810. https://doi.org/10.1016/j.apenergy.2019.113810.

[27] Marchese M, Heikkinen N, Giglio E, Lanzini A, Lehtonen J, Reinikainen M. Kinetic study based on the carbide mechanism of a Co-Pt/γ-Al₂O₃ Fischer-Tropsch catalyst tested in a laboratory-scale tubular reactor. Catalysts 2019;9:717. https://doi.org/10.3390/catal9090717.

[28] Tjaden B, Gandiglio M, Lanzini A, Santarelli M, Järvinen M. Small-scale biogas-SOFC plant: technical analysis and assessment of different fuel reforming options. Energy Fuels 2014. https://doi.org/10.1021/ef500212j.

[29] Raynal L, Bouillon PA, Gomez A, Broutin P. From MEA to demixing solvents and future steps, a roadmap for lowering the cost of post-combustion carbon capture. Chem Eng J 2011;171:742–52. https://doi.org/10.1016/j.cej.2011.01.008.

[30] Li K, Leigh W, Feron P, Yu H, Tade M. Systematic study of aqueous monoethanolamine (MEA)-based CO₂ capture process: techno-economic assessment of the MEA process and its improvements. Appl Energy 2016;165:648–59. https://doi.org/10.1016/j.apenergy.2015.12.109.

[31] Moioli S, Pellegrini LA, Gamba S. Simulation of CO₂ capture by MEA scrubbing with a rate-based model. Procedia Eng 2012;42:1651–61. https://doi.org/10.1016/j.proeng.2012.07.558.

[32] Vidal Vázquez F, Pfeifer P, Lehtonen J, Piermartini P, Simell P. V. Alopaeus, catalyst screening and kinetic modeling for CO production by high pressure and temperature reverse water gas shift for Fischer-Tropsch applications. Ind Eng Chem Res 2017;56:13262–72. https://doi.org/10.1021/acs.iecr.7b01606.

[33] Christensen KO. Steam Reforming of Methane on Different Nickel Catalysts. Norwegian University of Science and Technology; 2005Hdl.handle.net/11250/248086.

[34] Tractebel, Engie, Hinicio, Study on Early Business Cases for H2 in Energy Storage and More Broadly Power To H2 Applications, 2017. http://www.hinicio.com/inc/uploads/2017/07/P2H_Full_Study_FCHJU.pdf%0Ahttp://www.fch.europa.eu/sites/default/files/P2H_Full_Study_FCHJU.pdf%0Ahttp://www.hinicio.com/file/2018/06/P2H_Full_Study_FCHJU.pdf.

[35] Hauch A, Brodersen K, Chen M, Mogensen MB. Ni/YSZ electrodes structures optimized for increased electrolysis performance and durability. Solid State Ionics 2016;293:27–36. https://doi.org/10.1016/j.ssi.2016.06.003.

[36] Zhang X, Song Y, Wang G, Bao X. Co-electrolysis of CO₂ and H₂O in high-temperature solid oxide electrolysis cells: recent advance in cathodes. J Energy Chem 2017;26:839–53. https://doi.org/10.1016/j.jechem.2017.07.003.

[37] Giglio E, Lanzini A, Santarelli M, Leone P. Synthetic natural gas via integrated high-temperature electrolysis and methanation: Part I - Energy performance. J Energy Storage 2015;2:64–79. https://doi.org/10.1016/j.est.2015.06.004.

[38] Zheng Y, Wang J, Yu B, Zhang W, Chen J, Qiao J, et al. A review of high temperature co-electrolysis of H₂O and CO₂ to produce sustainable fuels using solid oxide electrolysis cells (SOECs): advanced materials and technology. Chem Soc Rev 2017;46:1427–63. https://doi.org/10.1039/c6cs00403b.

[39] Kazempoor P, Braun RJ. Hydrogen and synthetic fuel production using high temperature solid oxide electrolysis cells (SOECs). Int J Hydrogen Energy 2015;40:3599–612. https://doi.org/10.1016/j.ijhydene.2014.12.126.

[40] Clausen LR, Butera G, Jensen SH. High efficiency SNG production from biomass and electricity by integrating gasification with pressurized solid oxide electrolysis cells. Energy. 2019:1117–31. https://doi.org/10.1016/j.energy.2019.02.039.

[41] Graves C, Ebbesen SD, Mogensen M, Lackner KS. Sustainable hydrocarbon fuels by recycling CO₂ and H₂O with renewable or nuclear energy. Renew Sustain Energy Rev 2011;15:1–23. https://doi.org/10.1016/j.rser.2010.07.014.

[42] Saeidi S, Nikoo MK, Mirvakili A, Bahrani S, Saidina Amin NA, Rahimpour MR. Recent advances in reactors for low-temperature Fischer-Tropsch synthesis: process intensification perspective. Rev Chem Eng 2015;31:209–38. https://doi.org/10.1515/revce-2014-0042.

[43] Van De Loosdrecht J, Botes FG, Ciobica IM, Ferreira A, Gibson P, Moodley DJ, Saib AM, Visagie JL, Weststrate CJ, Niemantsverdriet JWH. Fischer-Tropsch Synthesis: Catalysts and Chemistry Elsevier Ltd.; 2013. https://doi.org/10.1016/B978-0-08-097774-4.00729-4.

[44] Tucker CL, van Steen E. Activity and selectivity of a cobalt-based Fischer-Tropsch catalyst operating at high conversion for once-through biomass-to-liquid operation. Catal Today 2018. https://doi.org/10.1016/j.cattod.2018.12.049.

[45] Yang J, Ma W, Chen D, Holmen A, Davis BH. Fischer-Tropsch synthesis: a review of the effect of CO conversion on methane selectivity. Appl Catal A Gen 2014;470:250–60. https://doi.org/10.1016/j.apcata.2013.10.061.

[46] Luyben WL, Yu CC. Reactive distillation design and control. Wiley; 2008. https://doi.org/10.1002/9780470377741.

[47] Al Ashraf A, Al A. Aftab, Distillation Process of Crude Oil. Qatar University; 2012.

[48] Campanario FJ, Gutiérrez Ortiz FJ. Fischer-Tropsch biofuels production from syngas obtained by supercritical water reforming of the bio-oil aqueous phase. Energy Convers Manag 2017;150:599–613. https://doi.org/10.1016/j.enconman.2017.08.053.

[49] Stempien JP, Ni M, Sun Q, Chan SH. Thermodynamic analysis of combined solid oxide electrolyzer and Fischer-Tropsch processes. Energy 2015;81:682–90. https://doi.org/10.1016/j.energy.2015.01.013.

[50] Beil M, Beyrich W. Biogas upgrading to biomethane. Biogas Handb Sci Prod Appl 2013:342–77. https://doi.org/10.1533/9780857097415.3.342.

[51] Sun Q, Li H, Yan J, Liu L, Yu Z, Yu X. Selection of appropriate biogas upgrading technology-a review of biogas cleaning, upgrading and utilisation. Renew Sustain Energy Rev 2015;51:521–32. https://doi.org/10.1016/j.rser.2015.06.029.

[52] Brand CV. CO₂ Capture Using Monoethanolamine Solutions: Development and Validation of a Process Model Based on the SAFT-VR Equation of State. London: Imperial College; 2013.

[53] Economico MDS. D.M. 19 febbraio 2007 Approvazione, 2007.
[54] Huang Y, Zhang X, Zhang X, Dong H, Zhang S. Thermodynamic modeling and assessment of ionic liquid-based CO_2 capture processes. Ind Eng Chem Res 2014;53:11805–17. https://doi.org/10.1021/ie501538e.
[55] Zacchello B, Oko E, Wang M, Fethi A. Process simulation and analysis of carbon capture with an aqueous mixture of ionic liquid and monoethanolamine solvent. Int J Coal Sci Technol 2017;4:25–32. https://doi.org/10.1007/s40789-016-0150-1.
[56] Moioli S, Nagy T, Langé S, Pellegrini LA, Mizsey P. Simulation model evaluation of CO_2 capture by aqueous MEA scrubbing for heat requirement analyses. Energy Procedia 2017;114:1558–66. https://doi.org/10.1016/j.egypro.2017.03.1286.
[57] Storsæter S, Chen D, Holmen A. Microkinetic modelling of the formation of C_1 and C_2 products in the Fischer-Tropsch synthesis over cobalt catalysts. Surf Sci 2006;600f:2051–63. https://doi.org/10.1016/j.susc.2006.02.048.
[58] Dimitriou I, García-Gutiérrez P, Elder RH, Cuéllar-Franca RM, Azapagic A, Allen RWK. Carbon dioxide utilisation for production of transport fuels: process and economic analysis. Energy Environ Sci 2015;8:1775–89. https://doi.org/10.1039/c4ee04117h.
[59] Maitlis PM, de Klerk A. Greener Fischer-Tropsch processes for fuels and feedstocks, 2013. https://doi.org/10.1002/9783527656837.
[60] Wolf A, Jess A, Kern C. Syngas production via reverse water-gas shift reaction over a Ni-Al_2O_3 catalyst: catalyst stability, reaction kinetics, and modeling. Chem Eng Technol 2016;298:1040–8. https://doi.org/10.1002/ceat.201500548.
[61] Deka DJ, Gunduz S, Fitzgerald T, Miller JT, Co AC, Ozkan US. Production of syngas with controllable H_2/CO ratio by high temperature co-electrolysis of CO_2 and H_2O over Ni and Co-doped lanthanum strontium ferrite perovskite cathodes. Appl Catal B Environ 2019;248:487–503. https://doi.org/10.1016/j.apcatb.2019.02.045.
[62] Chein R-Y, Yu C-T. Thermodynamic equilibrium analysis of water-gas shift reaction using syngases-effect of CO_2 and H_2S contents. Energy 2017;141:1004–18. https://doi.org/10.1016/j.energy.2017.09.133.
[63] Gunduz S, Deka DJ, Ozkan US. Advances in high-temperature electrocatalytic reduction of CO_2 and H_2O. 1st ed. Elsevier Inc; 2018. https://doi.org/10.1016/bs.acat.2018.08.003.
[64] Leibbrandt NH, Aboyade AO, Knoetze JH, Görgens JF. Process efficiency of biofuel production via gasification and Fischer-Tropsch synthesis. Fuel 2013;109:484–92. https://doi.org/10.1016/j.fuel.2013.03.013.
[65] Monaco F, Lanzini A, Santarelli M. Making synthetic fuels for the road transportation sector via solid oxide electrolysis and catalytic upgrade using recovered carbon dioxide and residual biomass. J Clean Prod 2018;170:160–73. https://doi.org/10.1016/j.jclepro.2017.09.141.
[66] Samavati M, Santarelli M, Martin A, Nemanova V. Thermodynamic and economy analysis of solid oxide electrolyser system for syngas production. Energy 2017;122:37–49. https://doi.org/10.1016/j.energy.2017.01.067.
[67] De Klerk A. Fischer-Tropsch refining. Univ. Pretoria; 2012.
[68] Lillebø AH, Rytter E, Blekkan EA, Holmen A. Fischer-Tropsch synthesis at high conversions on Al_2O_3 supported Co catalysts with different H_2/CO levels (2017). https://doi.org/10.1021/acs.iecr.7b01801.
[69] Liu ZK, Ågren J, Hillert M. Application of the Le Chatelier principle on gas reactions. Fluid Phase Equilib 1996;121:167–77. https://doi.org/10.1016/0378-3812(96)02994-9.
[70] Schmidt P, Weindorf W, Roth A, Batteiger V, Riegel F. Power-to-liquids: potentials and perspectives for the future supply of renewable aviation. Umweltbundesamt 2016https://www.umweltbundesamt.de/en/publikationen/.
[71] Jarvis SM, Samsatli S. Technologies and infrastructures underpinning future CO_2 value chains: a comprehensive review and comparative analysis. Renew Sustain Energy Rev 2018;85:46–68. https://doi.org/10.1016/j.rser.2018.01.007.
[72] Rytter E, Borg Ø, Tsakoumis NE, Holmen A. Water as key to activity and selectivity in Co Fischer-Tropsch synthesis: Γ-alumina based structure-performance relationships. J Catal 2018;365:334–43. https://doi.org/10.1016/j.jcat.2018.07.003.
[73] Gavrilović Save, Blekkan. The effect of potassium on cobalt-based Fischer-Tropsch catalysts with different cobalt particle sizes. Catalysts 2019;9:351. https://doi.org/10.3390/catal9040351.
[74] Neill BJO, Jackson DHK, Lee J, Canlas C, Stair PC, Marshall CL, Elam W, Kuech TF, Dumesic JA, Huber GW. Catalyst design with atomic layer deposition (2015). https://doi.org/10.1021/cs501862h.
[75] Eskelinen P, Keskiväli L, Heikkinen N, Franssila S. Cobalt catalyst characterization and modification by atomic layer deposition for Fischer-Tropsch synthesis. Aalto University; 2019.
[76] Oviroh PO, Akbarzadeh R, Pan D, Coetzee RAM, Jen T-C. New development of atomic layer deposition: processes, methods and applications. Sci Technol Adv Mater 2019;20:465–96. https://doi.org/10.1080/14686996.2019.1599694.
[77] Abu Zahra MRM. Carbon dioxide capture from flue gas: development and evaluation of existing and novel process concepts, 2009. http://www.google.com/patents/US20110226010%5Cnhttp://repository.tudelft.nl/view/ir/uuid:6d1689f3-7b1a-4355-81b0-af3d19fae469/.